GL02215

MICROGEOPHYSICS CORPORATION

TUSCARORA
SEISMICITY
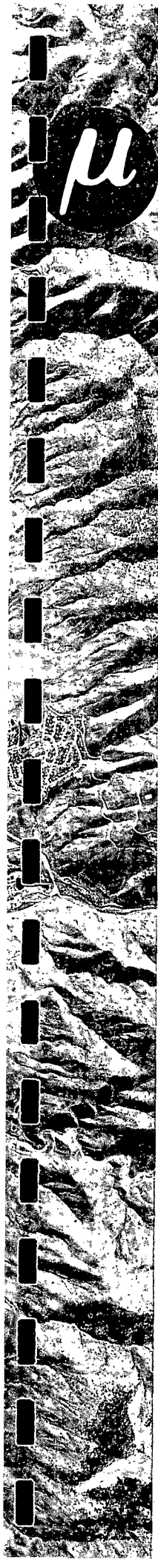
TUSCARORA SEISMICITY

MICROGEOPHYSICS

TABLE OF CONTENTS   PAGE

MICROGEOPHYSICS

LIST OF FIGURES

MICROGEOPHYSICS

LIST OF TABLES

MICROGEOPHYSICS

LIST OF PLATES

MICROGEOPHYSICS

1.0.0 INTRODUCTION

From September 10 to September 22, 1978, MicroGeophysics Corporation conducted a passive seismic survey in the area of Tuscarora, Nevada (see location and index map). Passive seismic mapping techniques have been important and useful for geothermal exploration. These seismic techniques are derived from classical seismology and include microearthquake mapping, and measurement of acoustic rock properties. Both of these methods will be discussed below.

1.1.0 Microearthquake Mapping
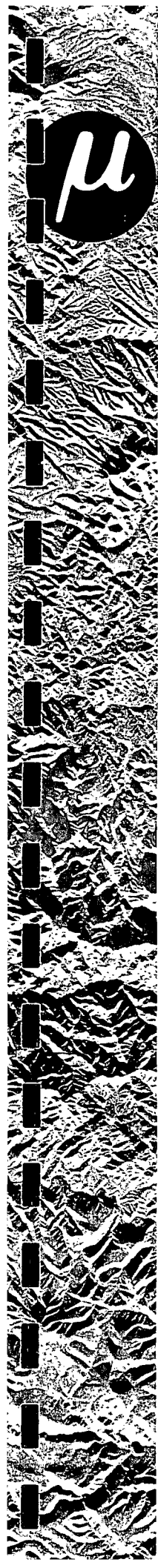
Microearthquakes are natural, discrete, seismic disturbances. These disturbances are the result of catastrophic rock failure under stress. Microearthquakes and microearthquake systems of varying activity levels have been observed at every proven geothermal area. Microearthquakes and the implied contemporary tectonism are a necessary ingredient for a commercial geothermal occurrence (Lange and Westphal, 1969; Ward and Bjornson, 1971; Ward and Jacob, 1971; Hamilton and Muffler, 1972; Ward, 1972; Combs and Hadley, 1977). Microearthquake activity indicates that active tectonism is currently occurring, therefore the associated porosity and permeability are being augmented. The zone of increasing porosity and permeability can be an excellent geothermal target. The zone may contain either the reservoir itself or the circulation path for geothermal fluids. Of course the microearthquake method does not directly indicate sufficient temperature or sufficient water recharge for a commercial system.

MICROGEOPHYSICS

N

Scale 1:250,000

| 5 | 0 | 5 | 10 | 15 | 20 Statute Miles |

| 5 | 0 | 5 | 10 | 15 | 20 | 25 | 30 Kilometers |

NEVADA

SURVEY AREA

40°

• RENO

0   200

KM

36°

116°
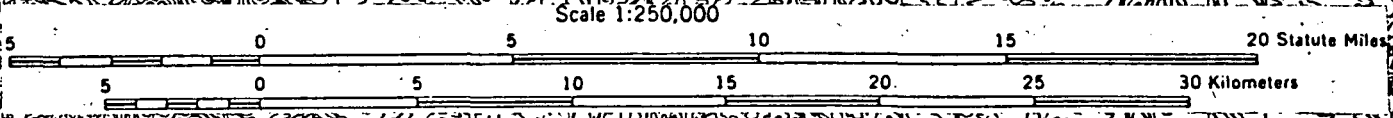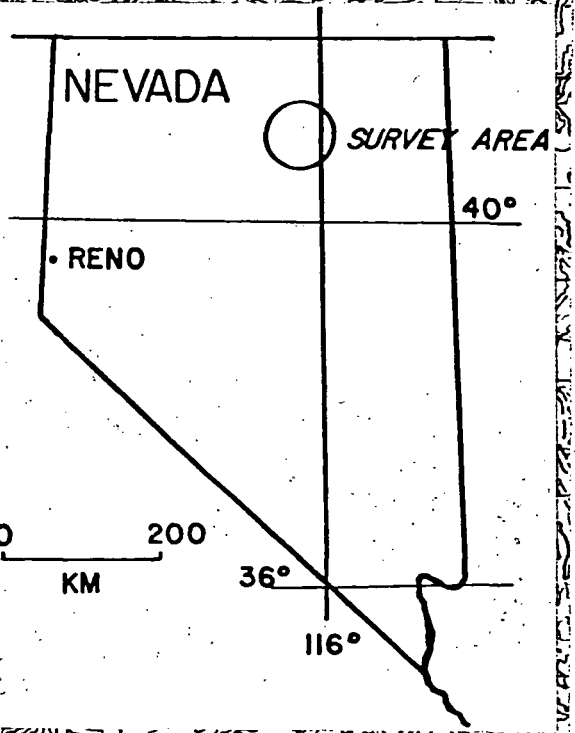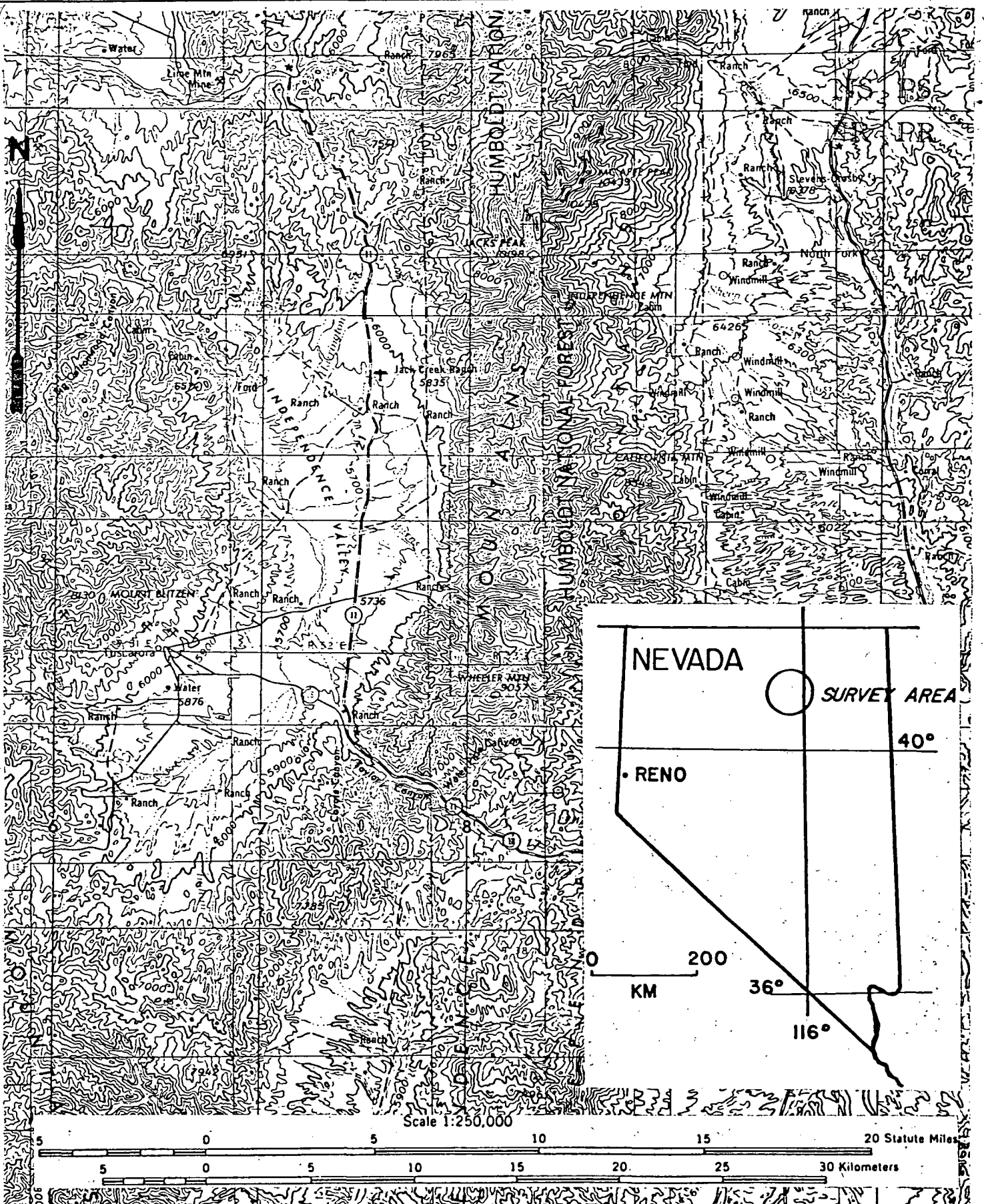
LOCATION AND INDEX MAP

FIGURE 1.1
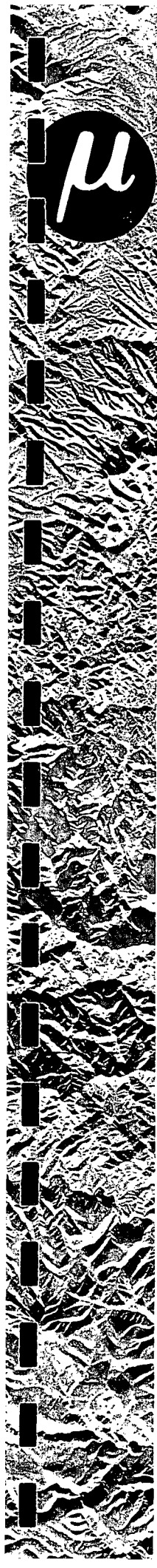
Mapping of discrete events for a geothermal area produces data about fault locations. First-motion studies produce data on the type and style of faulting and the direction of motion on faults. The statistics of occurrence of microearthquakes are used to compile a recurrence curve and to characterize and compare active geothermal areas. Some rock properties such as Poisson's Ratio can also be mapped utilizing local events. The location and style of faulting, characteristics of activity, and mapping of rock properties aid in the geologic understanding and delineation of a geothermal system.

1.2.0 Rock Properties, P-Wave Delay

A change in temperature will change the velocities of S- and P-waves in rock slightly. The acoustic attenuation of sound waves in rock is more dependent on temperature than is velocity. Fractures in rock change the S- and P-wave velocity in rock to some degree. The effect can be most easily observed as changes in the ratio of S-wave to P-wave velocities. Thus, if attenuation and the velocities can be measured with some degree of confidence, it may be possible to isolate two of the requirements for a commercial reservoir; i.e., high fracture porosity and rock at elevated temperatures.

Reliable sources of S- and P-wave energy include regional earthquakes (distances greater than 200 km) and industrial-blasting events. These events and the high frequencies in some teleseisms are useful if phases can be separated into either S- or P-wave type of energy. A frequency-dependent transfer function between

each station and a master station can then be calculated. The amplitude spectrum of this function will indicate the amount of attenuation taking place and the phase spectrum will indicate the time shift of the data. These values can be compared to a homogeneous model and anomalous areas isolated.

If S- and P-wave arrivals can be analyzed separately, both velocities and attentuation for the two modes of propagation can be calculated. If both S-wave and P-wave delay are calculated, a nonlinear combination of the two velocities, i.e., Poisson's Ratio can be calculated. The Poisson's Ratio can be used to delineate areas of anomalous fractures. The variation of Poisson's Ratio with fracturing, however, is not straight forward. For example, the Poisson's Ratio will decrease in general as fracturing increases. However, Poisson's Ratio may increase if the fractures are fluid filled.

The following report includes a section on geology and historical seismicity, and sections on operations, microearthquakes and rock properties. The final section is a summary of the conclusions from each of the previous sections. Appendices include information about the instruments used, the methods used, and a log of the microearthquakes detected.

INTRODUCTION BIBLIOGRAPHY

Combs, J. and David Hadley, 1977, Microearthquake Investigation of the Mesa Geothermal Anomaly, Imperial Valley, California, Geophysics, Vol. 42, No. 1, pp. 17-33.

Hamilton, R.M. and L.J.P. Muffler, 1972, Microearthquakes at the Geysers Geothermal Area, California, JGR, Vol. 77, No. 11, pp. 2081.

Lange, E., T.V. McEvelly and W.H. Westphal, 1969, Microearthquakes at the Geysers, Sonoma County, California, JGR, Vol. 74, pp. 4377.

Ward, P.L., 1972, Microearthquakes: Prospecting Tool and Possible Hazard in the Development of Geothermal Resources, Geothermics, Vol. 1, No. 1, pp. 3.

Ward, P.L. and S. Bjornson, 1971, Microearthquakes, Swarms and Geothermal Areas of Iceland, JGR, Vol. 76, No. 17, pp. 3953.

Ward, P.L. and R.H. Jacob, 1971, Microearthquakes: In the Ahnuachapan Geothermal Field, El Salvador, Central America, Science, Vol. 173, pp. 328.

2.0.0 HISTORICAL SEISMICITY AND GEOLOGY

2.1.0 Historical Seismicity

Figure 2.1 is a plot of the historical seismicity for Nevada in- *Utah*
cluding years 1940 to 1974 (NOAA). The area near Tuscarora has

not experienced any nearby macroearthquake activity in the 30

years observation period.

2.2.0 Geologic Setting

The Tuscarora prospect is situated in Northern Nevada approxi-

mately 60 miles north to Elko, Nevada.

The stratigraphy of the area is comprised of a sequence of

Paleozoic sediments in contact with large bodies of Cenozoic

volcanics mainly comprised of rhyolitic valcanics. The fault

style is complex with thrust fault and normal faulting.

The Jack Creek fault striking nearly north-south is a dominent

feature within the area of interest. A second fault system

strikes east by northeast and may constitute a major fault direc-

tion. Figure 2.2 is a generalized geology map for the area.

UTAH
HISTORICAL SEISMICITY
1965-1974

SCALE 1:1000000

10 0 10 20 30 40
miles
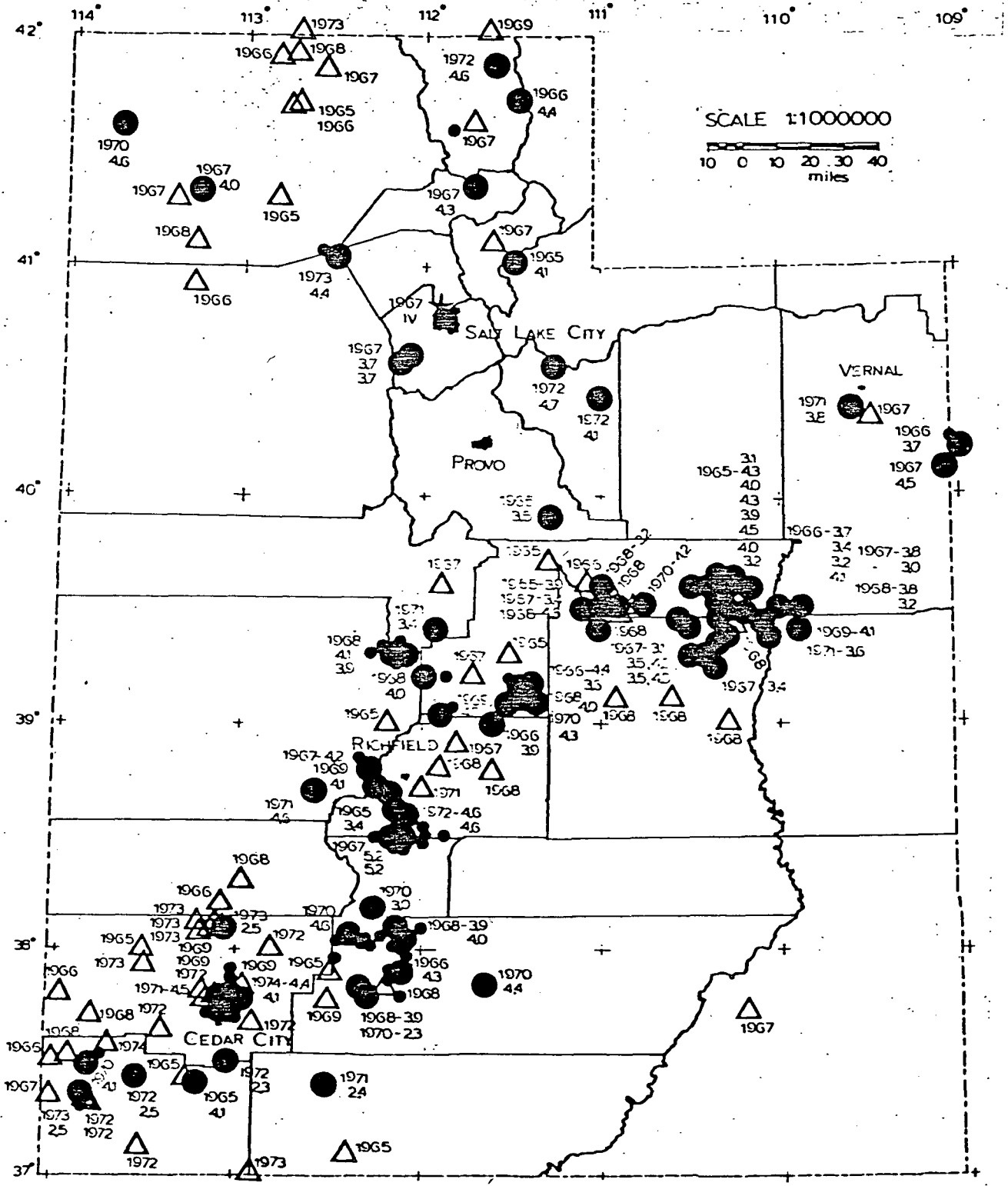
LEGEND

△ 1967   EPICENTER

● 1965   EPICENTER, MAIN SHOCK
 4.0   YEAR, MAGNITUDE

★ 1968-VI FELT REPORT
           YEAR, INTENSITY

•   EPICENTER
           AFTERSHOCK

FIGURE 2.1

GEOLOGY & HISTORICAL SEISMICITY MAP
FIGURE 2.2

Scale 1:500,000

```
10        0        10        20        30        40        50 Kilometers
```

Contact

High-angle fault
Dashed where inferred or uncertain; dotted where concealed. Bar and ball on downthrown side

Low-angle fault
Dashed where inferred or uncertain; dotted where concealed. Sawteeth on upper plate
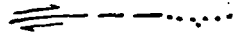
Strike-slip fault
Dashed where inferred or uncertain; dotted where concealed. Arrows indicate relative movement

Q	QUATERNARY
T	TERTIARY
C	CRETACEOUS

NEVADA

SURVEY AREA

40°

• RENO

0   200
KM

36°

116°
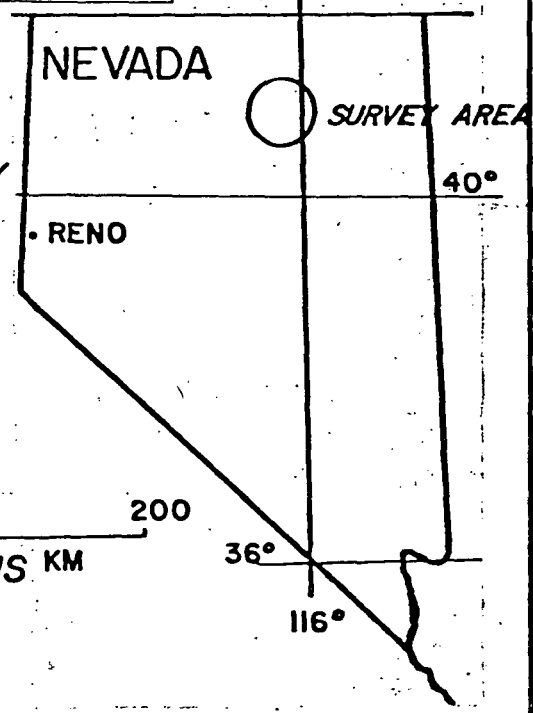
3.0.0 OPERATION

A passive seismic survey was conducted near Tuscarora, Nevada, from September 10 to September 22, 1978. Eleven days of recordings were obtained. Four to eight stations were operational on any one day (see operating schedule). The array was modified daily; a total of 30 stations were occupied. A station location map is shown in Figure 3.1. The station coordinates are listed in Table 3.1 and a detailed operations schedule is shown in Figure 3.2.

Each station of the passive seismic array consists of an MEQ-800-B smoked-paper recorder system with a companion digital magnetic tape recorder (see instrumentation appendix). Station locations were determined by considerations of access, specific array geometry and uniform coverage of the target area. Once a nominal station location was available, the location with the highest gain was selected. Where hard rock outcrops were available, the seismometer was cemented to the outcrop and then covered by soil to eliminate possible wind noise. When hard rock was not available the seismometer was buried from one to two feet within the soil. The data quality was generally good with less than five percent loss due to wind or cultural noise.
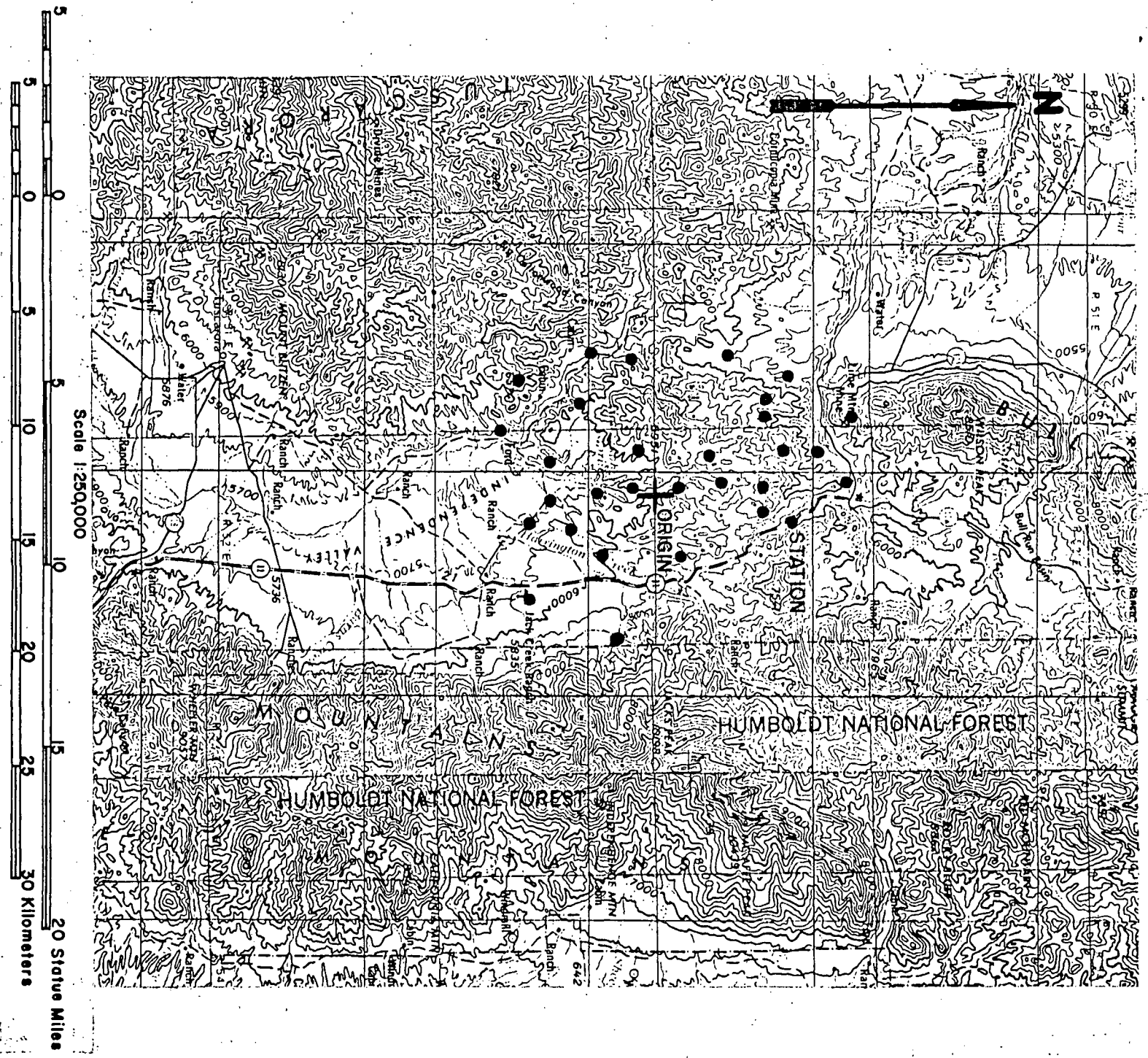
STATION LOCATION MAP
FIGURE 3.1

Scale 1:250,000

HUMBOLDT NATIONAL FOREST

HUMBOLDT NATIONAL FOREST

TABLE 3.1

STATION COORDINATES

STATION	X (km)	Y (km)	Z (km)
1	0.30	−6.25	0.25
1A	−4.65	−3.27	0.33
2	0.75	−3.90	0.29
3	−3.69	−7.30	0.21
4	−5.32	−6.25	0.32
5	−1.13	−1.55	0.30
6	5.65	−2.41	0.47
6A	1.75	−3.14	0.34
6B	−0.68	0.65	0.44
7	3.23	−6.19	0.29
8	−1.18	−3.19	0.26
8A	−3.00	−1.23	0.39
9	−2.34	−5.32	0.33
10	0.56	5.60	0.36
10A	1.91	1.00	0.48
10B	0.49	4.15	0.50
11	−1.07	8.00	0.24
11A	−2.86	6.68	0.27
11B	−2.86	5.22	0.53
11C	−1.22	4.16	0.54
11D	−1.12	2.78	0.45
12	−4.12	8.14	0.40
12A	−6.12	5.56	0.34

12B	-4.37	4.45	0.45
12C	-2.65	1.84	0.50
13	-7.20	3.13	0.28
14	-6.90	-3.50	0.21
14A	-6.50	-0.77	0.21
14B	-5.06	4.42	0.47

Station coordinates X, Y, and Z are kilometers

+X East

+Y North

Altitude datum is 1.5 km above sea level.

Origin is at longitude 116° 06.73' West, and latitude 41° 29.51' North.

OPERATIONAL SCHEDULE

FIGURE 3.2

4.0.0 MICROEARTHQUAKES

4.1.0 Introduction

The following section of this report concerns the microearth-
quakes detected during the 11-day passive seismic survey near
Tuscarora, Nevada. Microearthquakes occurred sporatically
during the 11-day survey. Included within the microearthquake
section of this report are discussions of the detection thres-
hold, velocity model, hypocenters, event occurrence statistics,
estimated strain release and a fracture-area map, first-motion
studies, and Poisson's Ratio map.

The section concludes with an interpretation of the microearth-
quake data presented.

4.2.0 Observations

4.2.1 Detection Threshold

The detection-threshold distance is defined as the largest hypo-
central distance at which a given magnitude earthquake will pro-
duce a trace displacement on the detecting instrument of at least
2 mm. Therefore, any event within the detection-threshold dis-
tance would be detected on at least one station if the event
exceeds the magnitude for which the detection-threshold distance
is calculated. The detection-threshold distance for Richter
magnitudes -1.0 and 0.0 are 4 and 7 km from each station. A
magnitude -0.5 event occurring within the Tuscarora survey area
would have been detected during the 11-day survey.

4.2.2 Velocity Model

The velocity model used to locate the microearthquakes has the form of a linear increase of velocity with depth. This model has two parameters; an initial velocity at the datum and a rate of change of velocity with depth. The value of these two parameters is adjusted to produce the best least-square fit to the measured time arrivals of the microearthquakes. In this case, the velocity model that produced the best fits was a linear-increase-with-depth velocity model with an initial velocity of 3.5 km/sec and an acceleration of 0.14 km/sec/km. Figure 4.1 shows the resulting velocity model. Also shown on Figure 4.1 is a layered velocity model as reported by Hill and Pakiser (1966). The layered model agrees favorablely with the derived linear increase of velocity with depth model.

4.2.3 Hypocenters

Plate 4.1 illustrates the hypocenters located. A list of all located events is contained in Table 4.1. Plate 4.2 shows cross sections.

4.2.4 Occurrence Statistics

Figures 4.2 and 4.3 are plots of the number of events versus the time of occurrence. Figure 4.2 plots the number of events versus the day of the survey. Of the total 108 events, 103 occurred on day 260 (September 17, 1978). Figure 4.3 details the occurrence of events by the hour within day 260. The occurrence of events splits into two groups, one at 5 hours to 11 hours, with 58 events and the second at 14 hours to 16 hours with a total of 45 events.

VELOCITY (KM/SEC)
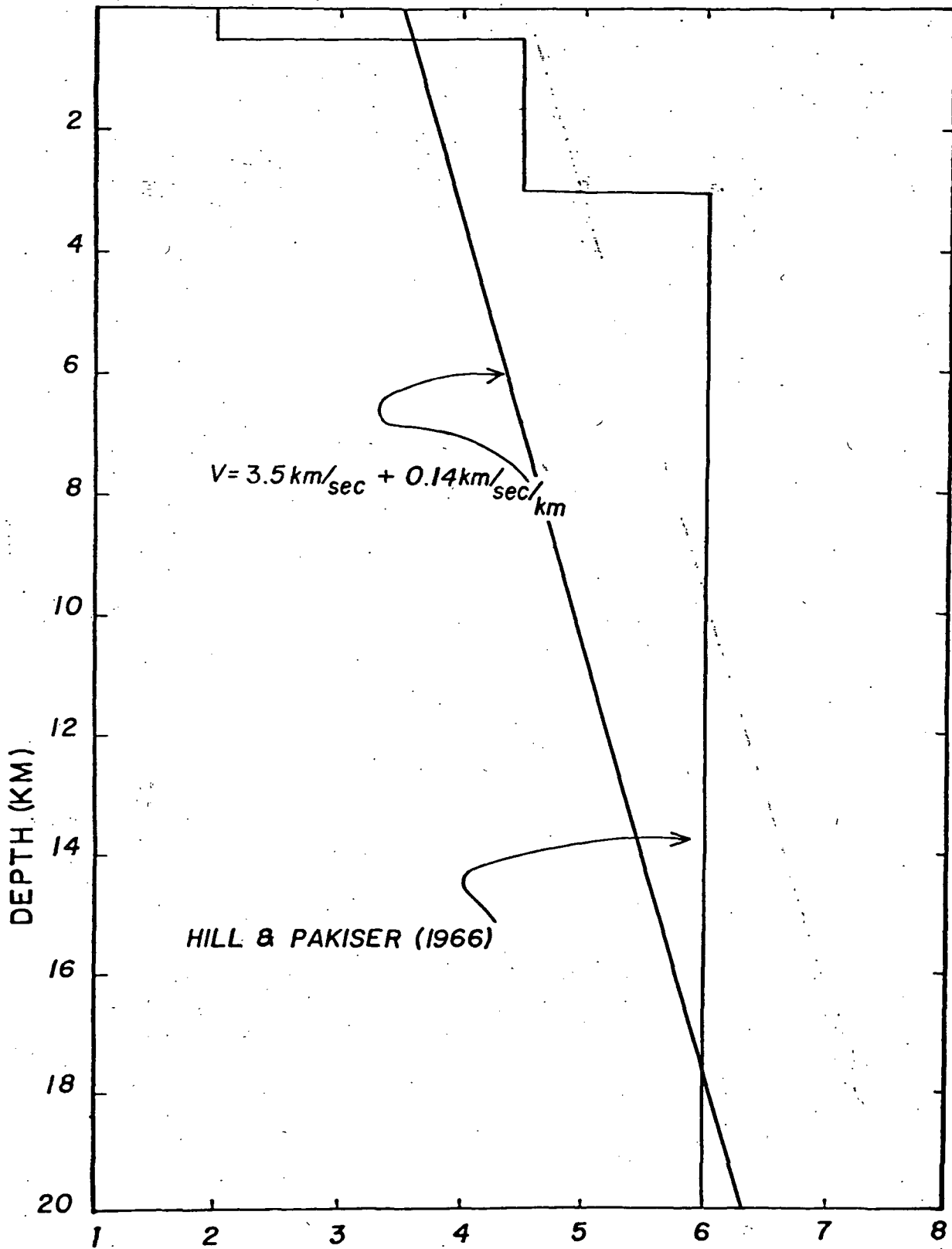
$V = 3.5\,km/_{sec} + 0.14\,km/_{sec}/_{km}$

HILL & PAKISER (1966)

VELOCITY MODEL
TUSCARORA

FIGURE 4.1

TABLE 4.1
EVENT LOG
Tuscarora, Nevada

DAY	UCT ORIGIN TIME	X (km)	Y (km)	Z (km)	MAG
254	16:03:43.72	7.5	-5.8	9.3	0.15
255	23:50:10.57	7.1	-5.2	5.7	1.31
256	18:37:33.56	0.4	4.8	4.7	1.47
260	05:03:33.96	2.4	-11.2	4.0	0.25
260	05:04:12.97	9.3	-4.4	0.0	0.45
260	05:12:26.44	1.5	-1.2	7.3	0.55
260	05:14:09.52	6.3	-6.1	10.9	1.34
260	05:15:41.21	6.5	-1.9	9.0	0.45
260	05:18:40.79	7.2	-5.0	10.0	0.03
260	05:19:01.14	5.7	-11.3	8.6	0.89
260	05:23:25.54	4.8	-2.6	10.2	-0.05
260	05:24:29.21	2.2	5.1	9.7	0.45
260	05:24:45.55	2.4	-0.8	5.7	0.50
260	05:25:42.59	6.2	-6.8	9.8	0.47
260	05:27:16.24	4.5	0.1	5.6	0.53
260	05:29:26.02	9.0	-3.5	10.7	0.07
260	05:45:33.14	3.5	-0.6	5.8	0.05
260	05:46:22.91	4.8	-1.7	8.8	-0.24
260	05:47:47.65	4.6	-3.0	9.6	0.33
260	05:52:12.69	2.7	-3.4	9.6	0.52
260	05:52:19.39	1.6	-1.0	10.0	0.23
260	05:57:37.60	2.5	-2.2	7.5	0.06
260	06:03:10.88	1.9	-1.0	5.1	-0.25
260	06:03:41.80	4.3	-1.5	8.8	-0.22
260	06:08:48.97	4.8	-3.8	9.9	1.38
260	06:09:44.63	11.8	-1.1	0.0	0.33

DAY	UCT ORIGIN TIME	X (km)	Y (km)	Z (km)	MAG
260	06:11:26.10	4.5	-3.0	10.0	0.07
260	06:11:48.05	5.5	-5.7	9.3	1.78
260	06:13:38.54	5.0	-2.7	9.4	0.25
260	06:16:58.00	8.7	1.1	7.7	0.51
260	06:17:53.06	7.9	-3.9	11.2	1.13
260	06:24:22.95	4.4	3.6	4.5	0.29
260	06:24:54.02	6.0	-7.1	8.7	0.94
260	06:29:32.82	9.9	-0.4	8.6	0.54
260	06:37:16.65	4.3	2.1	9.0	0.94
260	06:50:58.18	7.8	-3.5	10.6	1.54
260	06:52:31.37	4.2	-5.9	3.4	0.05
260	06:56:27.57	4.5	-2.5	9.5	-0.23
260	07:01:02.32	1.7	2.7	3.8	-0.43
260	07:01:55.97	1.3	2.5	8.3	0.38
260	07:12:27.00	4.5	-3.2	9.9	0.46
260	07:14:42.03	5.2	-3.2	7.2	-0.27
260	07:14:56.51	7.5	-8.3	13.9	-0.17
260	07:49:36.05	4.7	-2.5	10.9	0.53
260	07:54:38.85	1.3	1.7	7.7	-0.01
260	07:55:25.14	-4.2	-2.5	10.4	0.43
260	07:57:18.89	5.0	-2.8	10.3	-0.38
260	08:59:01.80	4.1	-2.0	9.5	0.74
260	09:38:40.92	6.4	-10.5	0.0	-0.53
260	09:51:40.02	13.7	-0.4	0.0	0.09
260	10:34:34.40	1.8	5.0	14.3	0.45
260	14:44:43.47	1.7	-1.5	7.8	0.27
260	14:46:03.71	9.7	-11.8	6.0	0.04
260	14:47:56.53	3.7	1.7	3.8	0.28
260	14:50:05.13	4.2	5.4	2.0	-0.03

DAY	UCT ORIGIN TIME	X(km)	Y(km)	DEPTH Z(km)	MAG
260	14:51:41.02	7.8	-3.9	5.3	-0.07
260	14:52:41.93	9.2	-10.2	6.5	-0.48
260	14:54:38.23	4.0	-2.3	11.5	0.98
260	14:55:20.31	6.2	1.3	8.7	0.90
260	14:55:37.61	1.9	0.2	11.5	0.86
260	14:58:34.68	6.5	-4.3	3.2	0.08
260	14:58:58.53	4.0	1.3	10.3	0.14
260	15:00:29.94	7.8	-3.9	2.8	0.07
260	15:00:52.27	7.7	-5.2	8.2	0.36
260	15:01:13.43	4.1	-7.0	4.5	0.92
260	15:01:39.73	3.4	-3.7	10.0	0.45
260	15:01:57.06	2.8	-5.7	11.2	1.18
260	15:02:51.08	0.8	1.7	9.2	0.95
260	15:03:24.62	9.9	-0.4	3.2	0.45
260	15:04:00.37	8.1	-7.5	12.4	0.76
260	15:04:38.78	6.3	5.0	3.2	0.36
260	15:06:44.25	7.5	-5.4	11.5	-0.15
260	15:06:59.84	10.2	3.6	0.0	1.14
260	15:08:43.27	-0.3	2.6	12.7	1.18
260	15:09:32.84	2.8	0.1	4.8	0.43
260	15:12:00.38	5.8	-10.4	6.7	0.14
260	15:16:25.17	7.5	-3.8	13.8	2.44
260	15:17:20.87	5.0	-0.2	8.9	1.18
260	15:18:33.69	1.7	3.2	8.5	0.41
260	15:41:15.02	4.2	-9.4	8.2	1.38
260	15:46:16.27	5.4	-4.7	4.2	0.90
260	15:50:01.87	3.5	-1.9	7.9	1.06
260	15:56:52.33	3.1	-1.3	7.9	0.31

Altitude datum is 1.5 km above sea level.

Origin is at longitude 116° 06.73' West, and

latitude 41° 29.51' North.

A characteristic of seismicity is the recurrence curve. The recurrence curve is a plot of the earthquake magnitudes versus the log of the cumulative number of earthquakes. This plot is typically a linear plot which indicates that for a given magnitude event a larger number of events will occur at a lesser magnitude. For a slope of -1.0, a ten-fold increase in the number of events will occur for a decrease in the magnitude of one.

The recurrence curve shown in Figure 4.4 is based on all the natural microearthquakes recorded at Tuscarora. An event is designated as a microearthquake when the event has a similar signature to other well recognized events. A b-slope of -1.0 is shown for comparison. A b-slope of -0.9 is considered an average value for worldwide seismicity.

Figures 4.5 and 4.6 are recurrence curves for the two populations of events previously described. Again each is shown with a comparison slope of -1.0.

As the magnitude decreases, the number of earthquakes detected no longer fits the straight line. This phenomena is caused by the decreased capability of the array to detect these very small (less than -1.0 magnitude) events. An empirical detection threshold is determined to be the approximate point that the recurrence curve departs significantly from linearity at small magnitudes. It can be seen from Figures 4.4, 4.5, and 4.6 that this point is about 0.0 magnitude. Therefore, it can be surmised that all events with magnitudes greater than 0.0 that occurred during this survey were detected.

MICROGEOPHYSICS
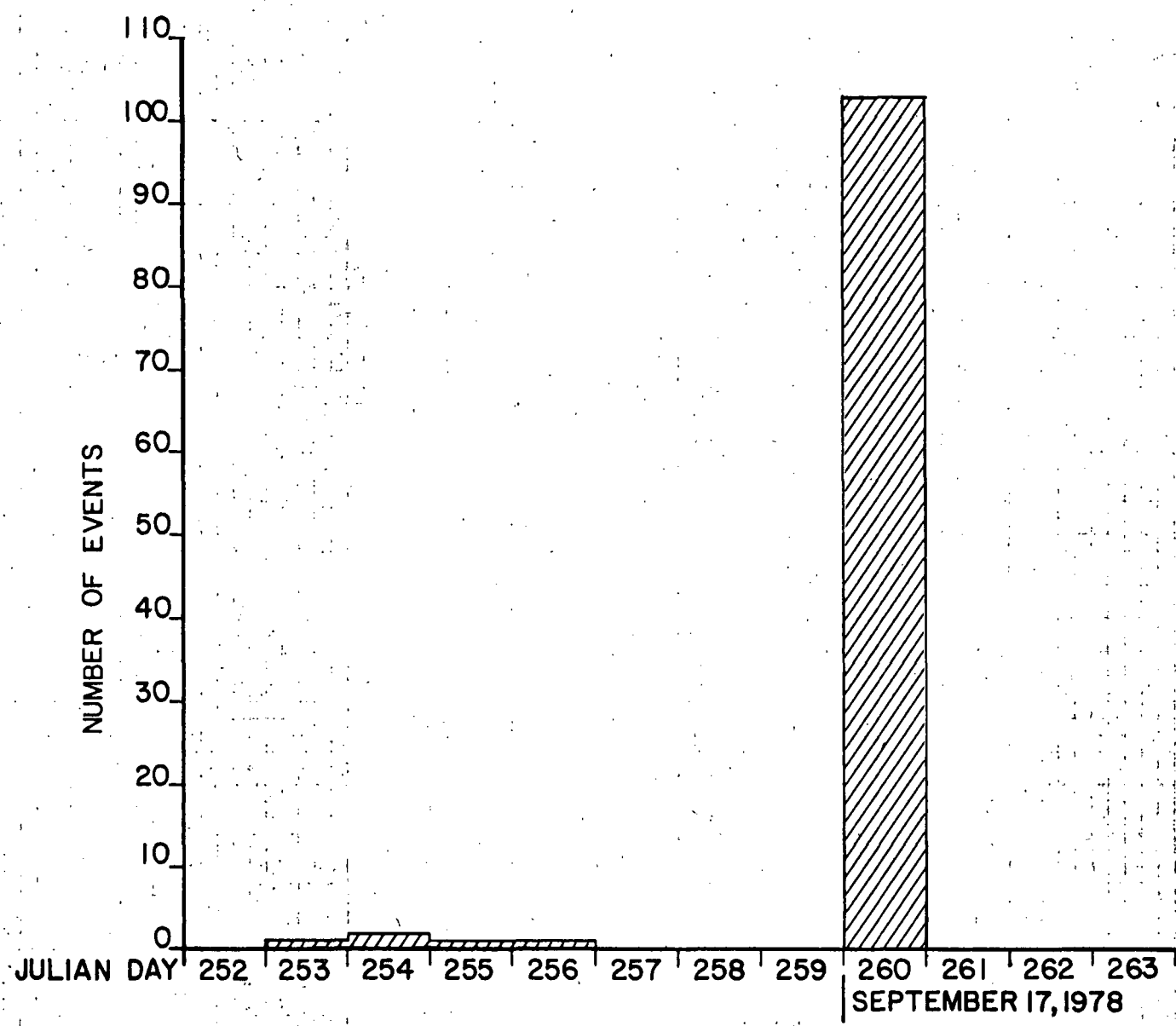
NUMBER OF EVENTS PER DAY

FIGURE 4.2
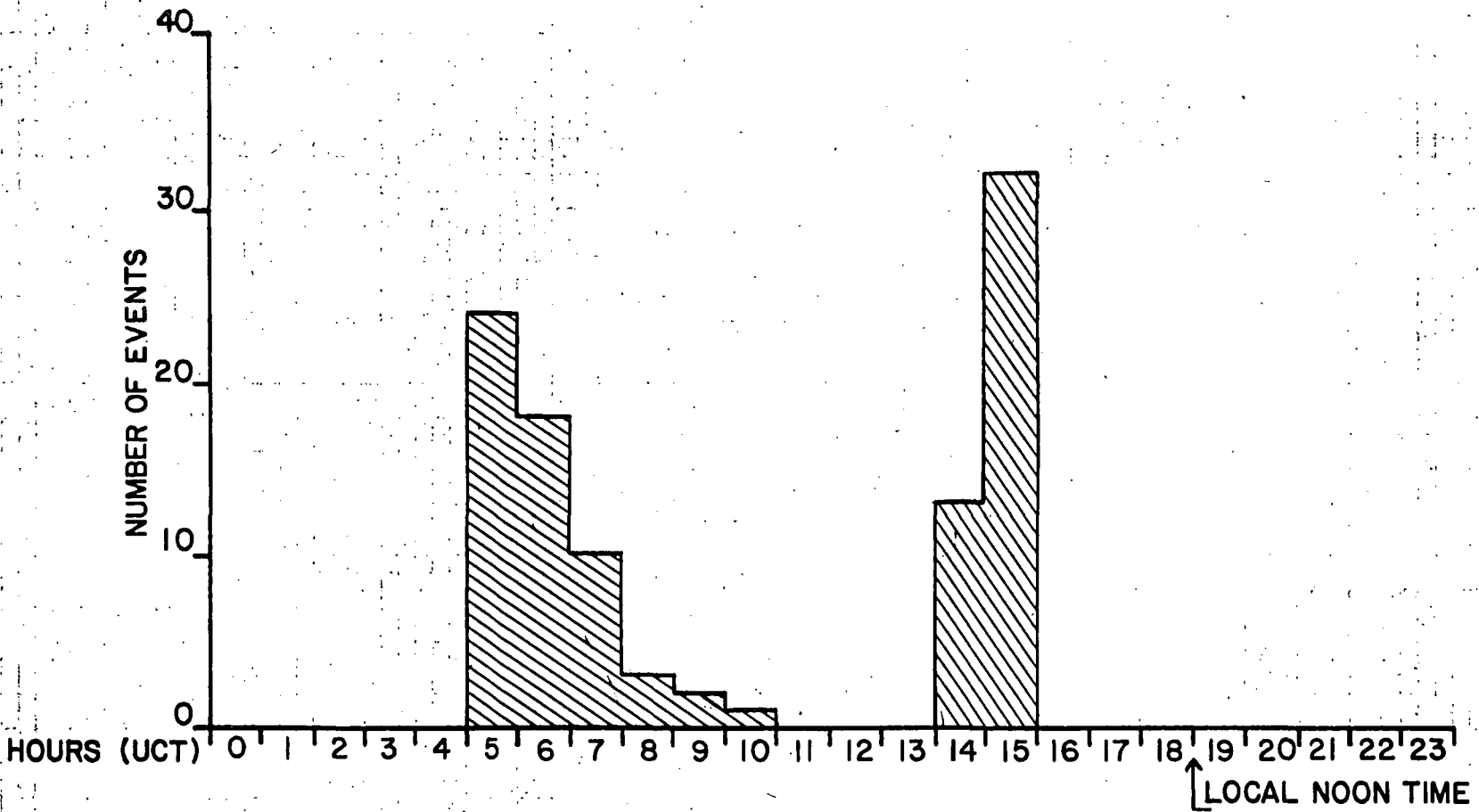
NUMBER OF EVENTS ON DAY 260 BY HOUR

FIGURE 4.3

EVENTS DAY 260 (I & II)
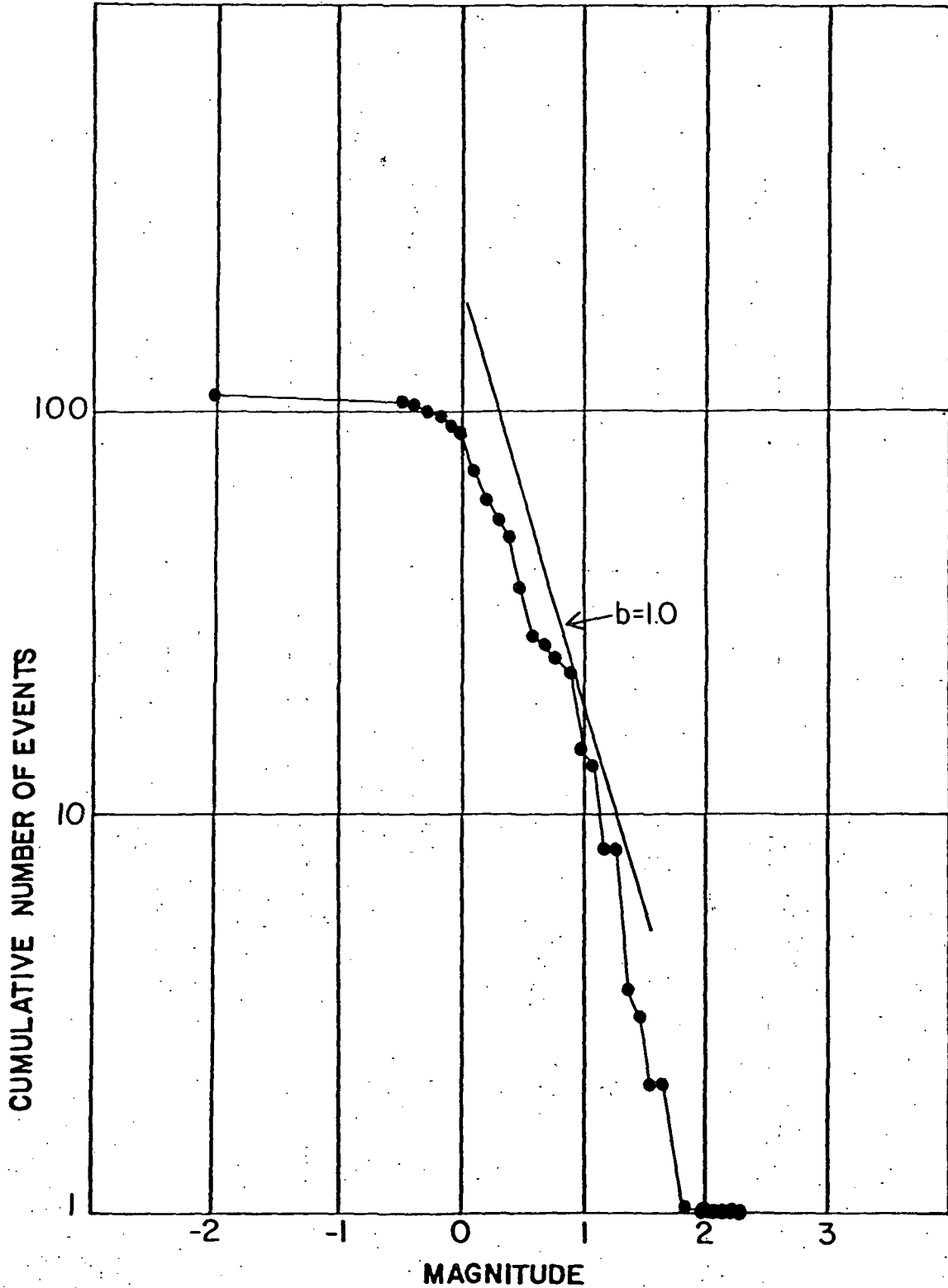
RECURRENCE CURVE

FIGURE 4.4

EVENTS DAY 260 10 Hrs - 1.3 Hrs (II)

DETECTION THRESHOLD

b = 1.0

CUMULATIVE NUMBER OF EVENTS
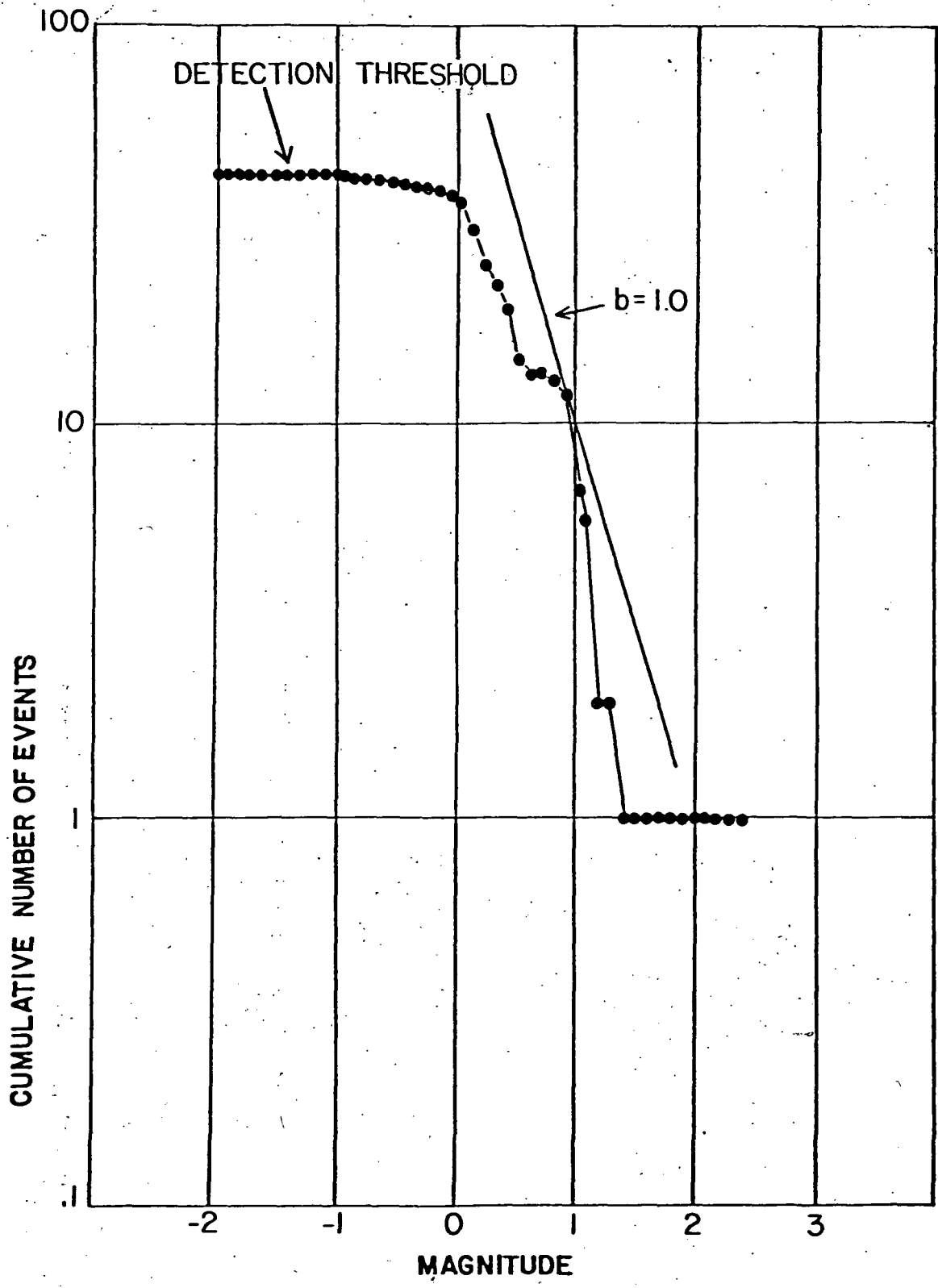
MAGNITUDE

RECURRENCE CURVE

FIGURE 4.5

EVENTS DAY 260 05 Hrs - 10 Hrs (I)
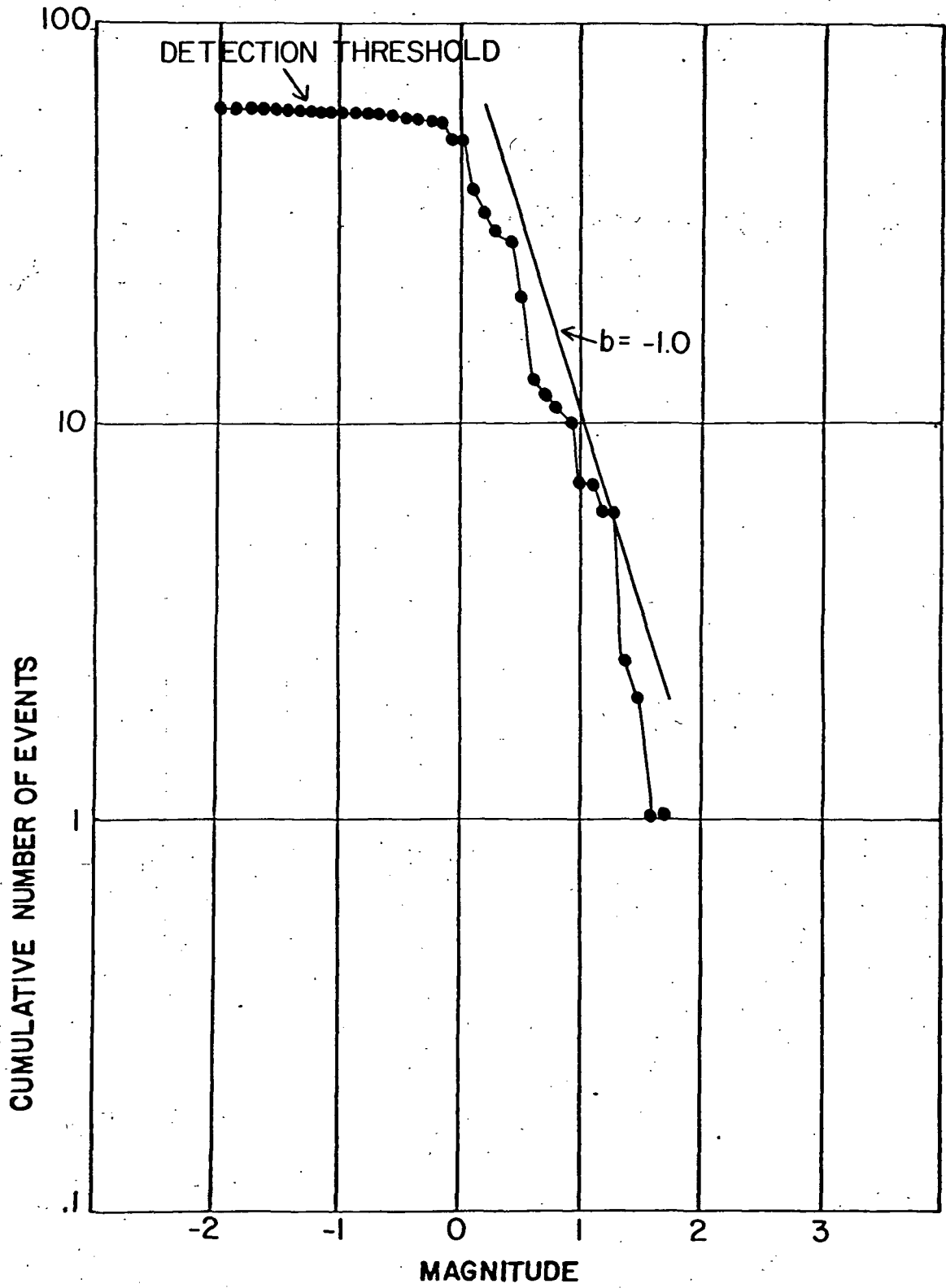
RECURRENCE CURVE

FIGURE 4.6

4.2.5 Strain Release

The relationship between strain release and magnitude established by Richter is:

$$LOG_{10} \ E = 9.4 + 2.14 \ m - 0.054 \ m^2$$

$$S = (E)^{\frac{1}{2}}$$

Where   E is the energy released in ergs

S is the amount of strain released in $(ergs)^{\frac{1}{2}}$

And   m is the magnitude (Richter).

The purpose for estimating strain release is to get an idea of the total energy and the total area of fracturing involved in the recorded seismic events.
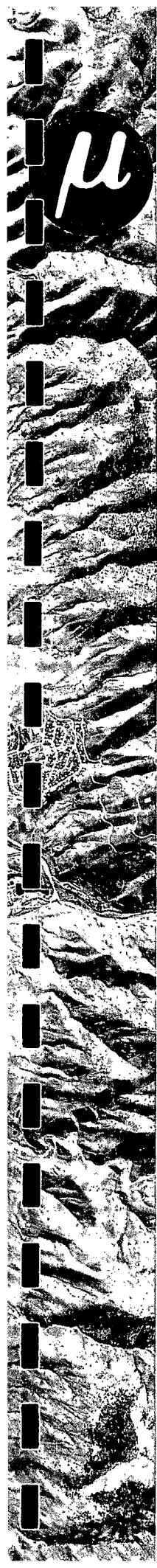
The strain release was calculated from assigned magnitudes. The total strain release for the locatable earthquakes is estimated to be 4.04×10^7 $(ergs)^{\frac{1}{2}}$ and corresponds to an equivalent amount of strain released from an earthquake of magnitude 2.92.

Plate 4.3 is a contour map of strain release in the survey area for the locatable earthquakes detected during this 11 day survey.

4.2.6 First-Motion Studies and Cross Sections

If seismographs record the direction of the first motion of the seismic energy at several azimuths from the event, the double-couple model of rock fracture will yield fault planes. A set of two orthogonal fault-plane solutions are determined; the preferred solution is denoted the fault-plane solution and the other, the auxiliary solution. Trends of hypocenters or

mapped geologic structures are helpful in determining the preferred solution.

Fault-plane solutions are shown in Figures 4.7 and 4.8. Each first motion is also shown in its hypocentral position on Figure 4.9. The first-motion plots are upper hemisphere projections of the source emergence angle. The direction of the first-motion, dilatation or compression, is plotted. Since none of the events were interior to the network, control of first-motion plots was not optimal.

4.2.7 Poisson's Ratio

If the S-P times for a specific event are plotted versus the P-phase arrival times at several stations, the resultant points will fall on a straight line if the subsurface is homogeneous. The point where this line crosses the S-P = 0 axis corresponds to the origin time of the earthquake. If inhomogeneities in the subsurface are suspected, and an origin is available from the computer fit to the data, a straight line can be drawn between the computed origin-time and the point corresponding to each station. This line defines the average crustal properties along the line from the earthquake location to the station. The crustal property defined is the P-wave to S-wave velocity ratio. The ratio is equal to the slope of the line plus 1.0. Such a plot is known as a Wadati plot (Figure 4.10). Individual-event Wadati plots were made for locatable events. It should be noted that the P-wave to S-wave

POISSON'S RATIO   1ST. MOTION

DAY   TIME (hr. min.)
260   14 54 ◓
255   23 50 ▣
260   05 18 ▲
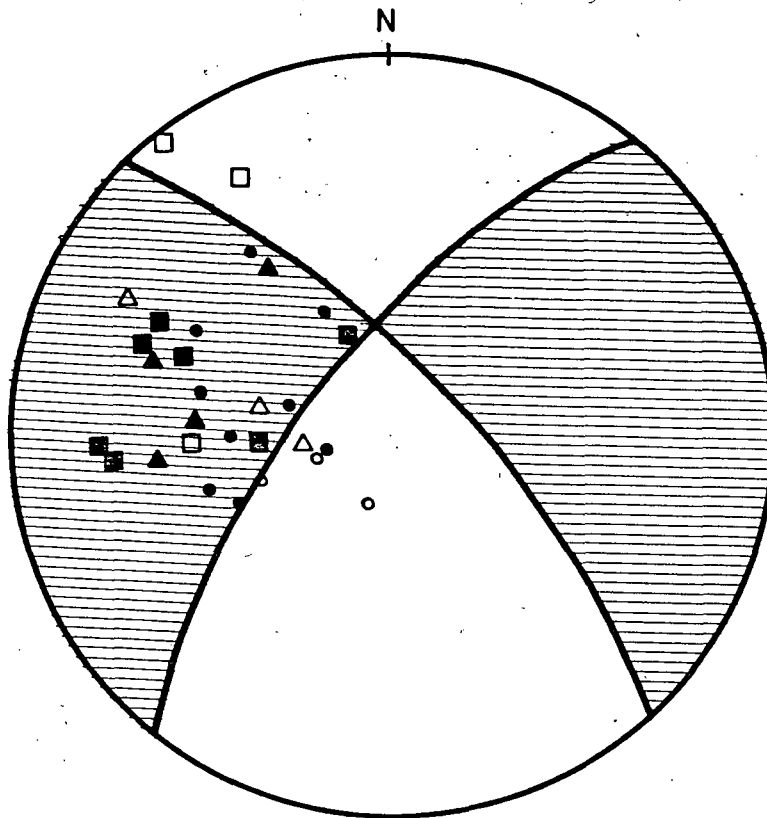
DAY   TIME (hr. min.)
260   07 14 ●
260   07 49 ■
260   08 59 ▲
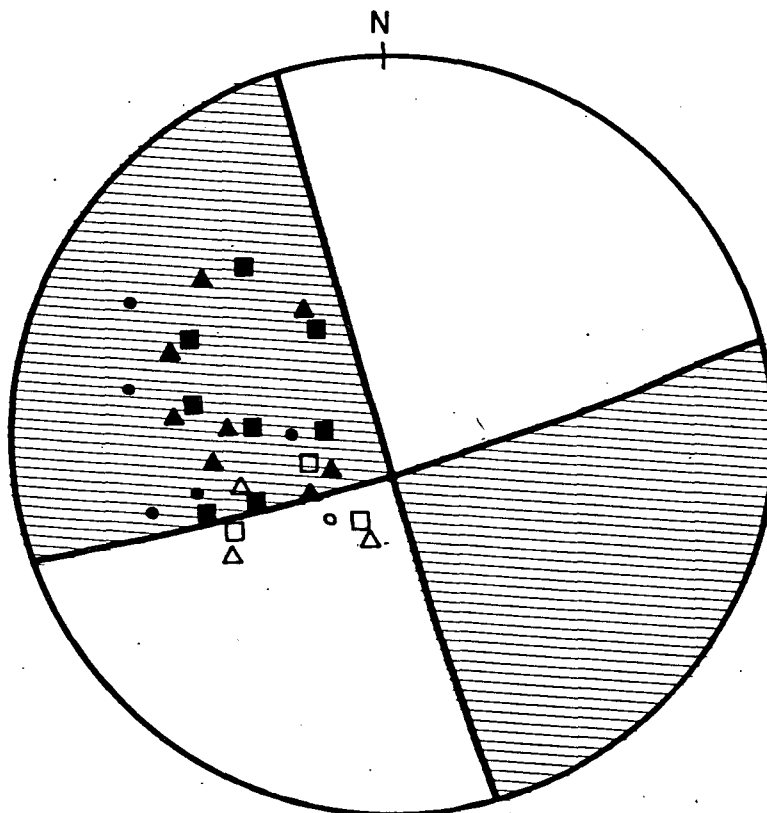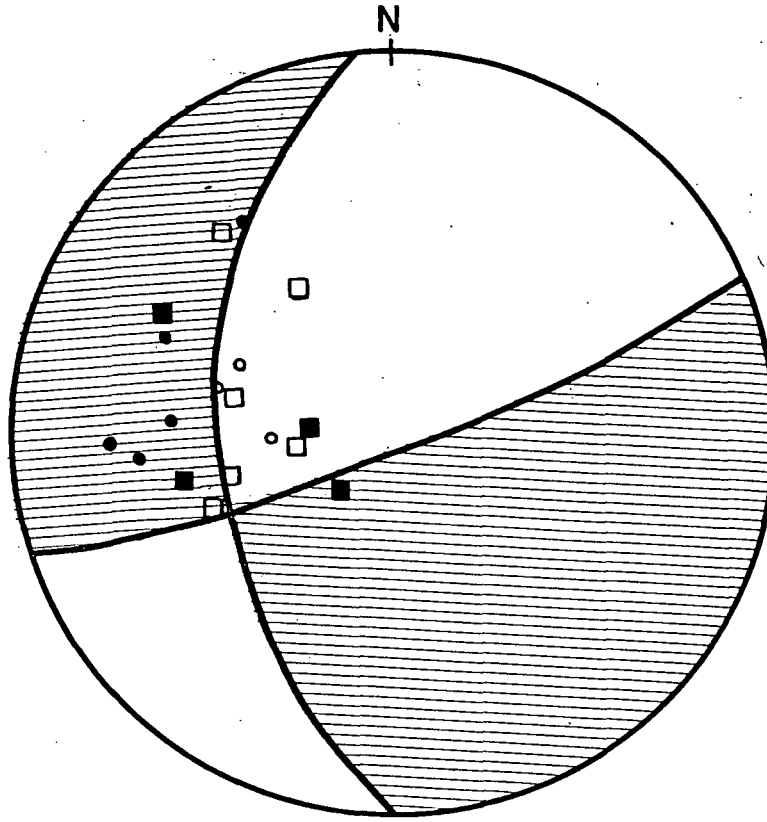
FIGURE 4.7

POISSON'S RATIO   1ST. MOTION

DAY   TIME (hr. min.)
260   15   00   •
260   07   57   ■

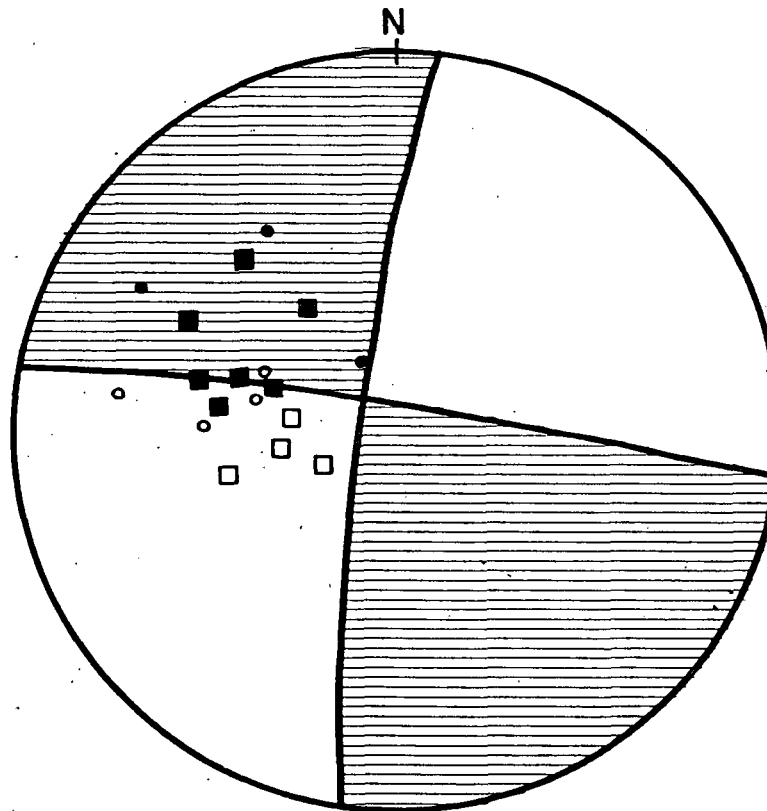DAY   TIME (hr. min.)
254   16   03   •
260   15   16   ■

FIGURE 4.8

FIRST MOTION MAP
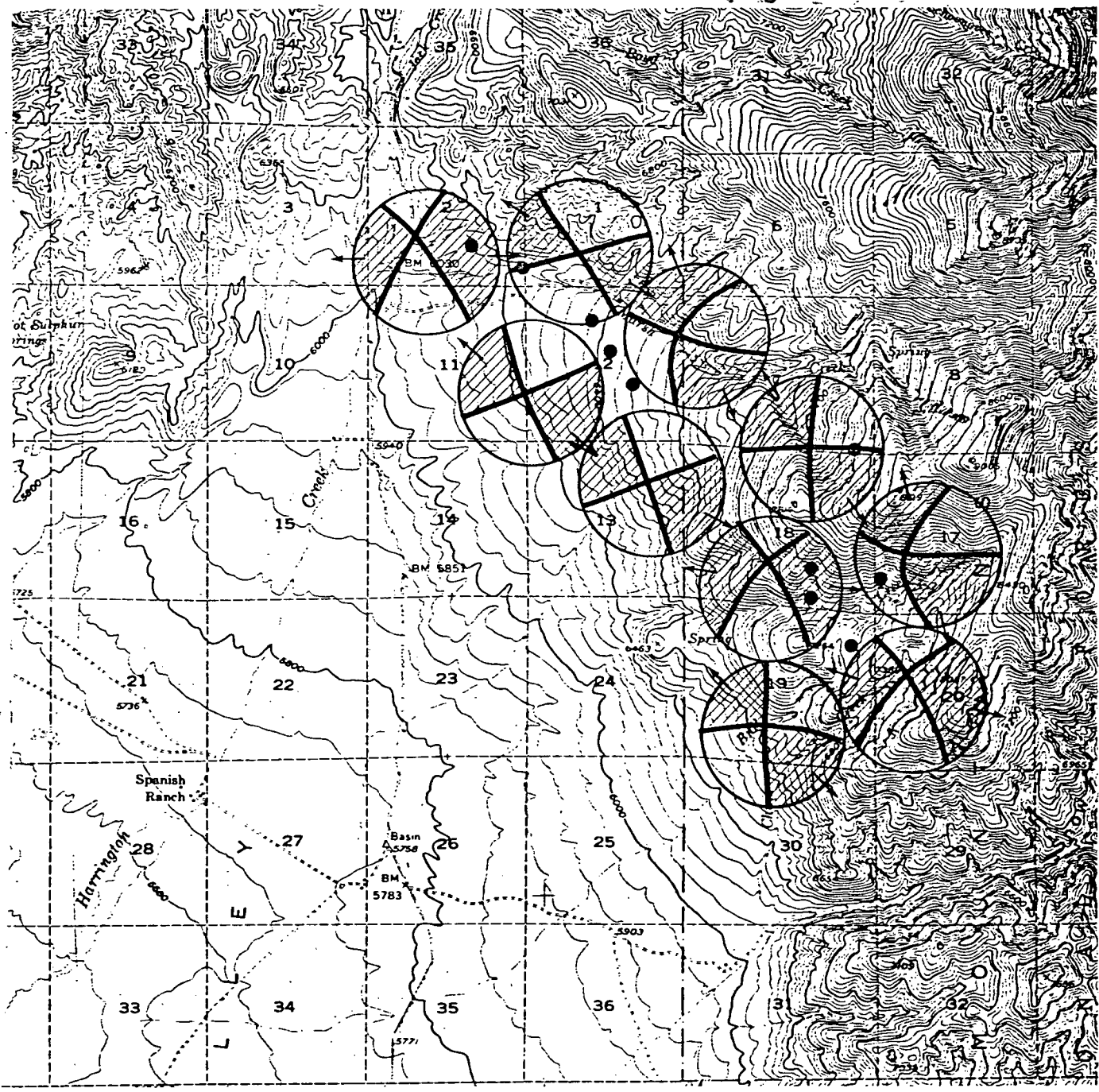
FIGURE 4.9

WADATI DIAGRAM
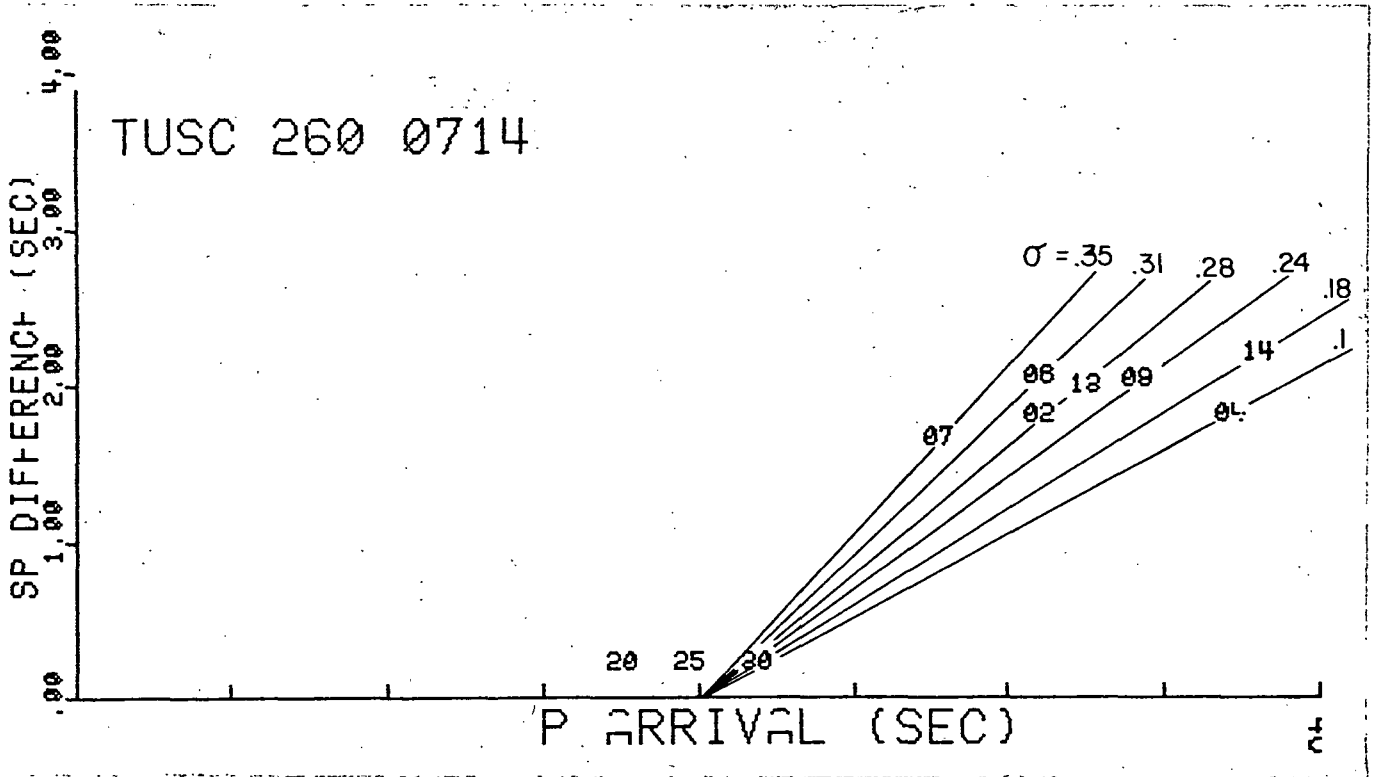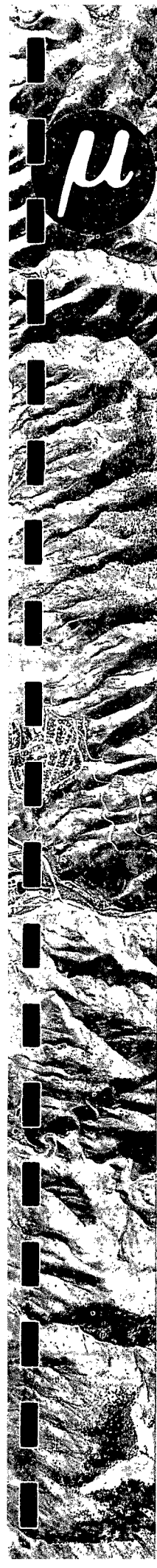
FIGURE 4.10

velocity ratio acquired for each event is correct only along
the raypath between the specific event and a particular
station. The purpose of the composite is to give average
values for the ratio under each station.
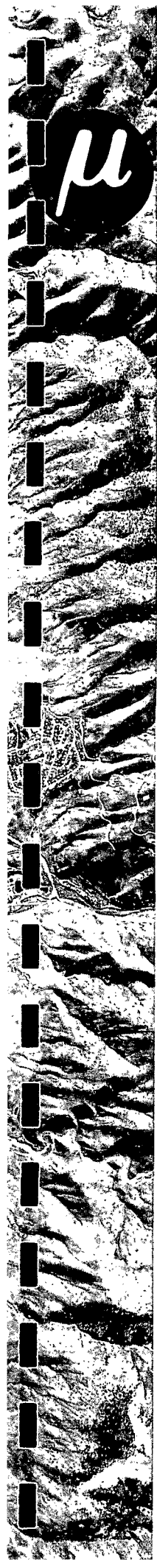
Another way of displaying the data is to convert the velocity
ratio to Poisson's Ratio. The equivalent Poisson's Ratio for
different slopes is also shown in Figures 4.7 & 4.8.

Once the Poisson's Ratio is determined for a specific raypath
joining a station to an event location, the projection of the
raypath on the surface is plotted on a map. The Poisson's
Ratio maps are shown in Plates 4.4 and 4.5. Most of the area
is near a normal Poisson's Ratio: 0.25 ± 0.05.

4.3.0   Interpretation

The area highlighted by this 11 day survey is the northeastern
basin boundary fault and the Jack Creek Fault area.

The microearthquake activity in this area indicates almost
vertical faulting with a slight dip to the south-southwest.
Although the first-motion studies are not well controlled, a
west-northwest fault trend should have a strong right-lateral
strike-slip component. Most of the activity appears to occur
at the intersection of the Jack Creek with the basin. The
strain release is highly dominated by the magnitude 2.44
earthquake which occurred at the northeast corner of the basin.

The Poisson's Ratio is primarily controlled by the very high σ
basin sediments which appear to be quite deep, in contrast to
the very low σ hard rock mountain range. However, again the
highest Poisson's Ratio is found at the north-northeasterly
corner of the basin.

MICROEARTHQUAKE BIBLIOGRAPHY

Hill, D.P., and L.C. Pakiser (1966), Custral structure between
    the Nevada Test Site and Boise, Idaho, from seismic-refraction
    measurements: in Earth Beneath the Continents, J.S. Steinhart,
    T.J. Smith, Editors, Geophys. Monogr. 10, Am. Geophys. Union,
    Washington, D.C., pp. 391-419.

5.0.0 P-WAVE DELAY

The P-wave delay technique can be used to delineate areas within a prospect where anomolously high velocity or low velocity material exists. A change in velocity can also result from a change in the structure. A deep section of sediments relative to near surface basement would result in a relative delay in the transmission of a teleseism. This resultant delay would not be a prduct of a change in velocity.

The P-wave delay technique can be used to delineate the geologic structure and therefore aid in the characterization of the geo-thermal potential of a prospect.

5.1.0 Procedure

Seven distant seismic events were recorded and used to generate residual travel times. Residual travel times are defined as the difference of the assumed model, which in this case is a plane wave transmission, and the observed wave front. The residuals are corrected for station elevation differences. The corrections in milliseconds are generated to datum by assuming a velocity and calculating, from the distance, the time correction. Since the origin time for the distance events is normally not well controlled, a relative travel time is used to generate the residuals. Realtive residuals are then used to generate a distance for a given velocity model. These distances from each station to the velocity interface surface is drawn. The interface surface highlights areas where either the velocity or structure is anomalous.

MICROGEOPHYSICS

5.2.0 Observations

Seven distant seismic events were recorded and used to construct the data base for the P-wave delay study. Table 5.1 lists these events. Each event is plotted as a pseudo refraction. The azimuth of the plane wave arrival, the phase velocity and the emergence angle if calculated from a data base provided by the NEIS (National Earthquake Information Service). The NEIS data base include the seismic event location, magnitude and origin time. All the pseudo refractions are shown in Figure 5.1 through 5.7.

TABLE 5.1

TELESEISM DATA

EVENT	TIME			LOCATION	
NUMBER	DAY	HR:MIN	DISTANCE	LATITUDE	LONGITUDE
1	258	11:39	60.0°	48.31°N	154.24°E
2	256	15:15	7.9°	37.21°N	116.21°W
3	257	02:36	89.0°	49.85°N	78.69°E
4	257	11:00	2.2°	42°53'54.1"N	113°48'34.2"W
5	259	15:35	107.0°	33.21°N	57.35°E
6	264	14:59	72.0°	66.43°N	85.84°E
7	259	23:38	89.0°	25.63°S	178.14°W

The P-wave attenuation studies included data from 5 events. These events are listed on Plate 5.4. This plate shows attenuation in terms of relative signal strength for each of the 5 event arrival azimuths. The relative signal strengths in db were calculated by comparing ground motion at each station at one frequency to the average signal amplitude. The signal frequency for the 5 teleseisms was near 2 Hz. Therefore a spectrum comparison was not possible. The results of the attenuation studies are not at this time comparable to the P-wave delay results.
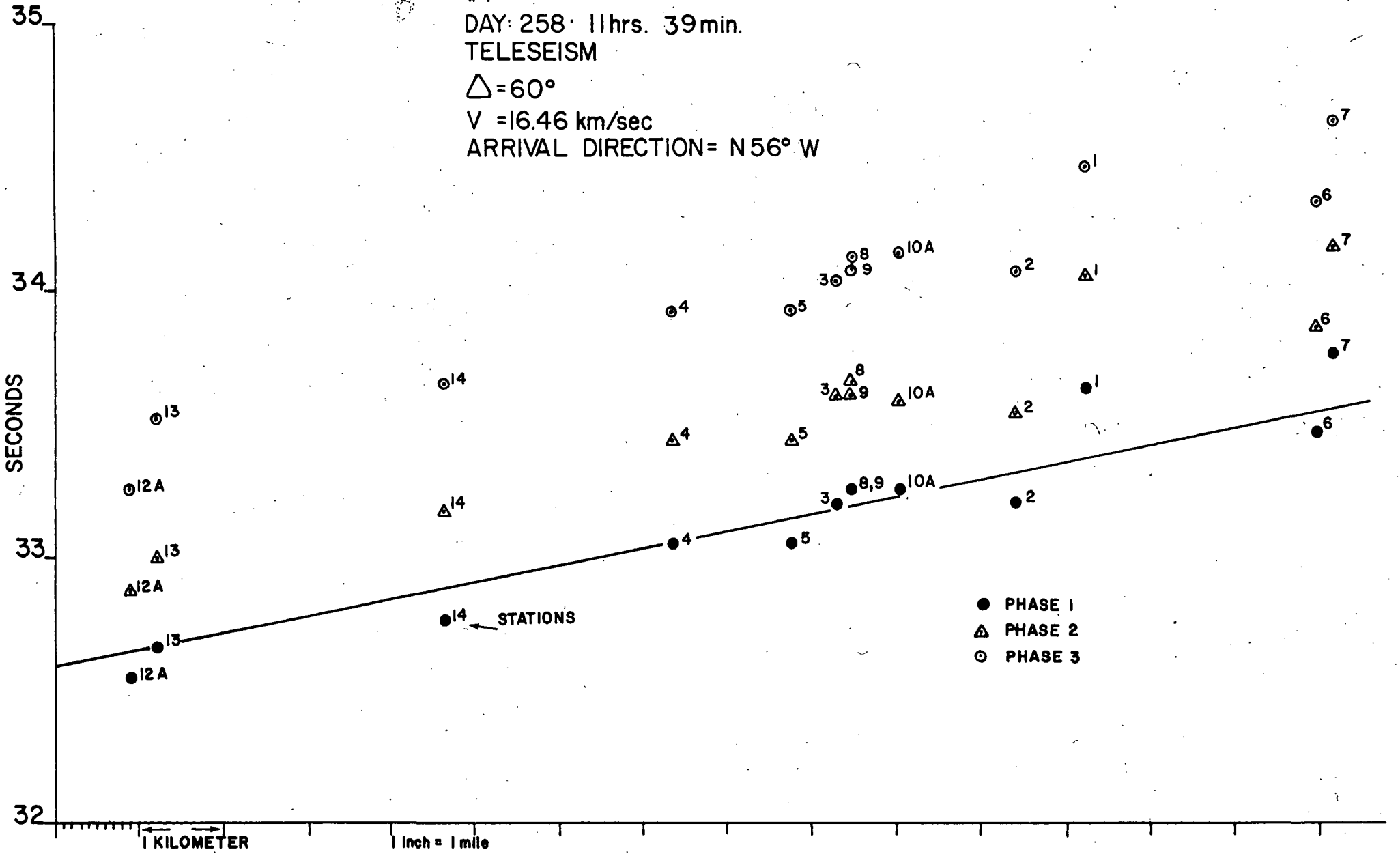
FIGURE 5.1

#2
DAY: 256   15 hrs.   15 min.
SOUTHERN NEVADA   (surface shot)
$\triangle = 7.9°$
V = 7.96 km/sec
ARRIVAL DIRECTION = SOUTH

SECONDS

STATIONS

PHASE I

1 KILOMETER   1 inch = 1 mile
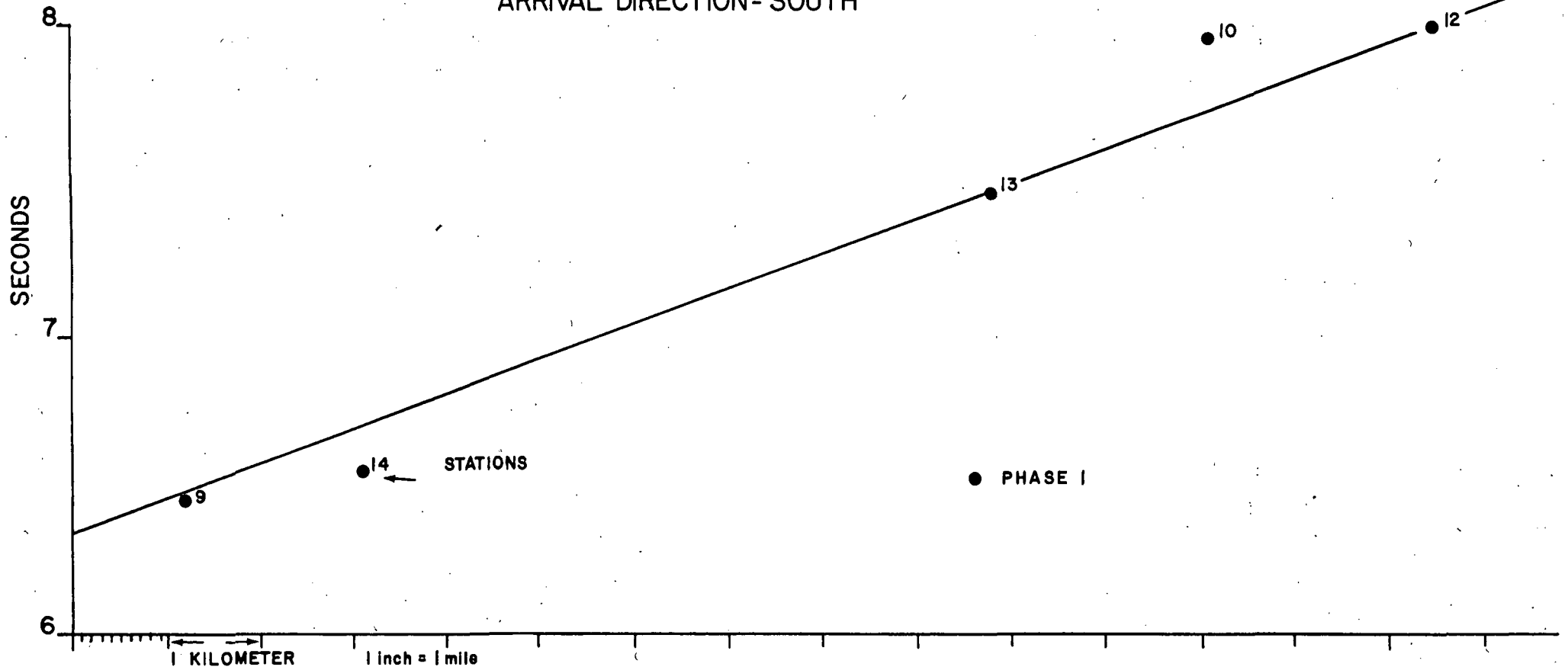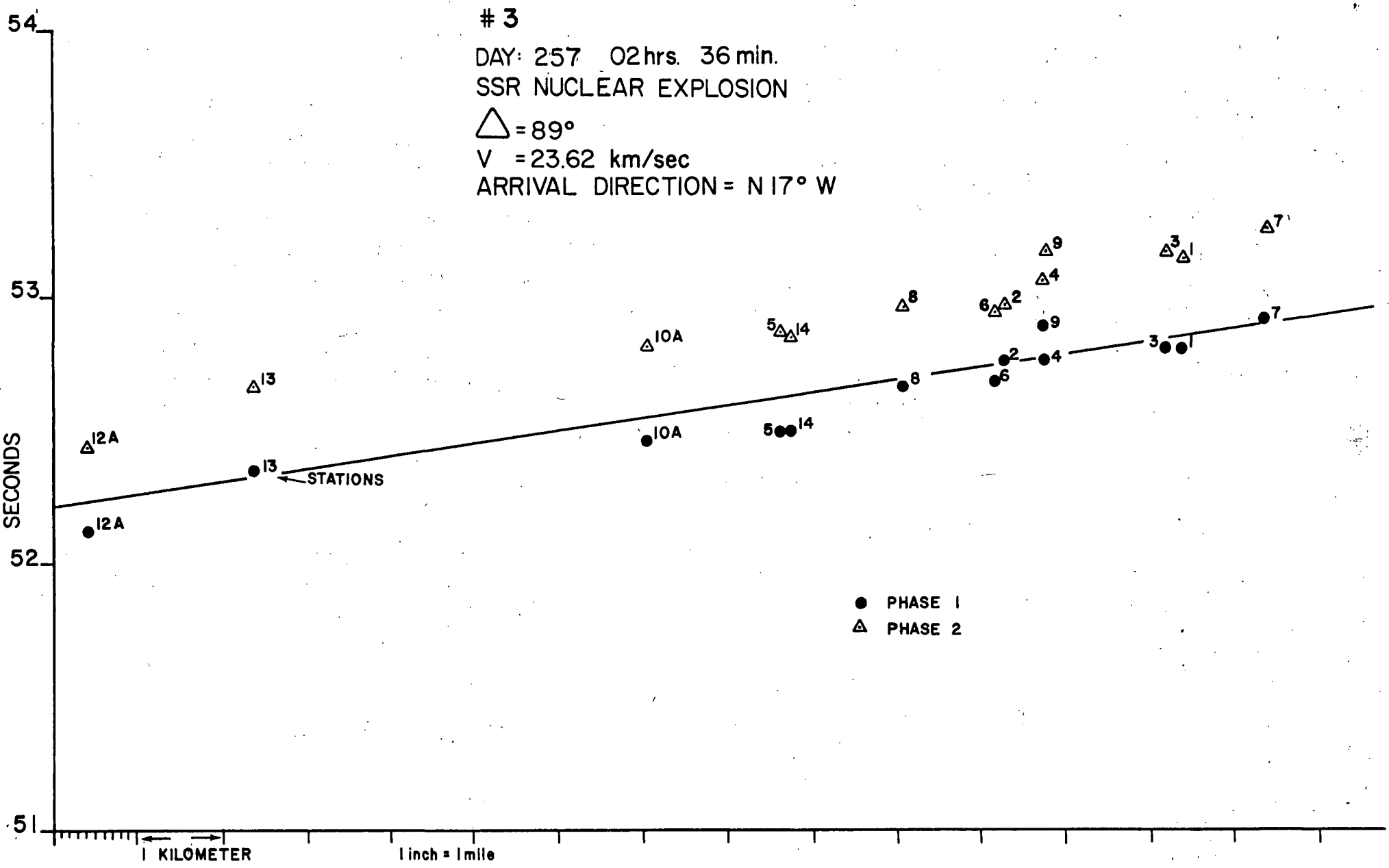
FIGURE 5.2

FIGURE 5.3

#4

DAY: 257 11hrs. 00min.
SHOT   SNRP
△ = 2.2°
V = 8.0 km/sec
ARRIVAL DIRECTION = N 50° E

SECONDS

STATIONS

● PHASE 1
△ PHASE 2
⊙ PHASE 3
△ PHASE 4

1 KILOMETER   1 inch = 1 mile

FIGURE 5.4

39

5
DAY: 259 15 hrs. 35 min.
IRAN
△= 107°

V = 25.3 km/sec
ARRIVAL DIRECTION = N 15° E
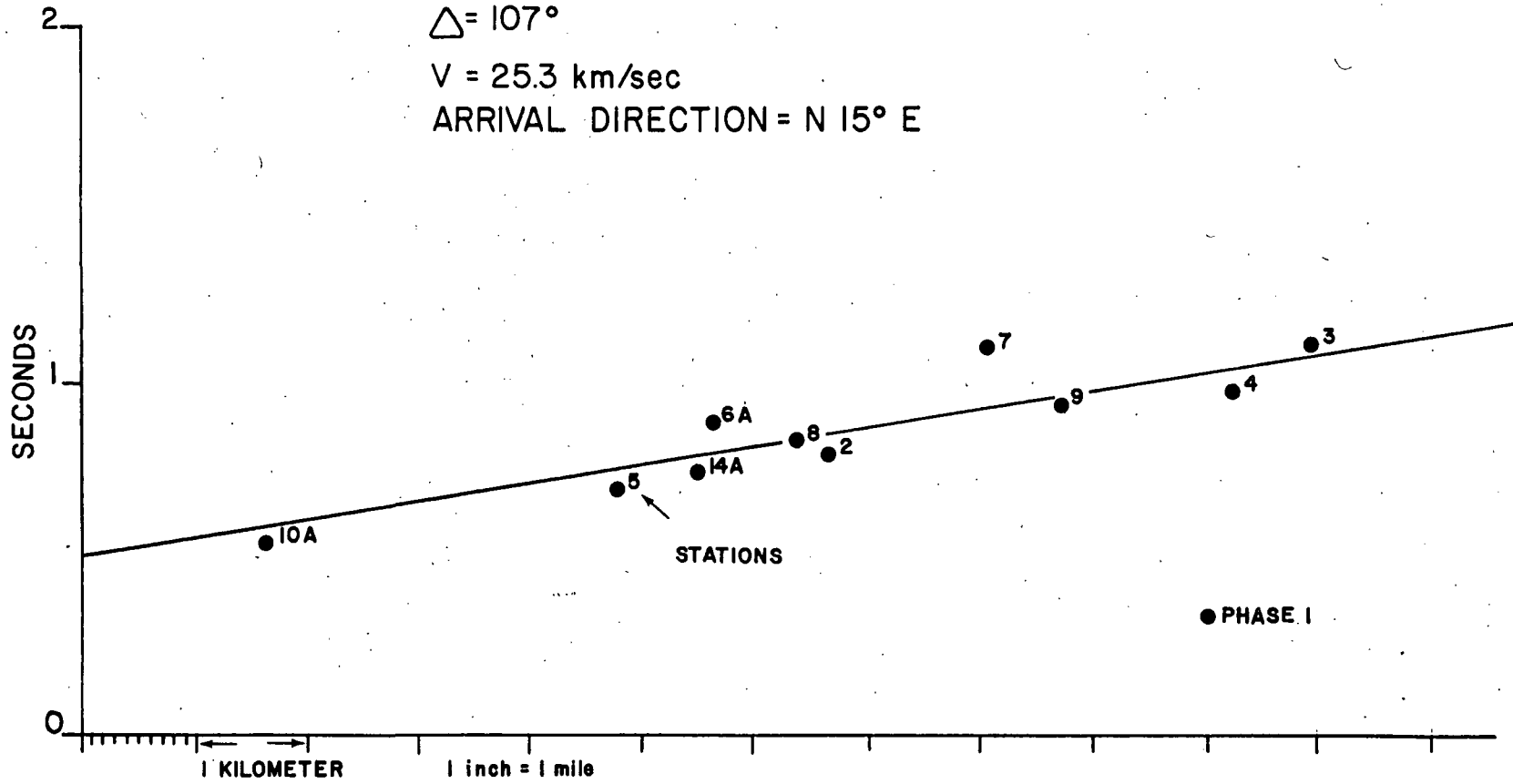
FIGURE 5.5

#6
DAY: 264   14hrs. 59min.
RUSSIA, SIBERIA
△ = 72°
V = 18.89 km/sec
ARRIVAL DIRECTION = N 10° W
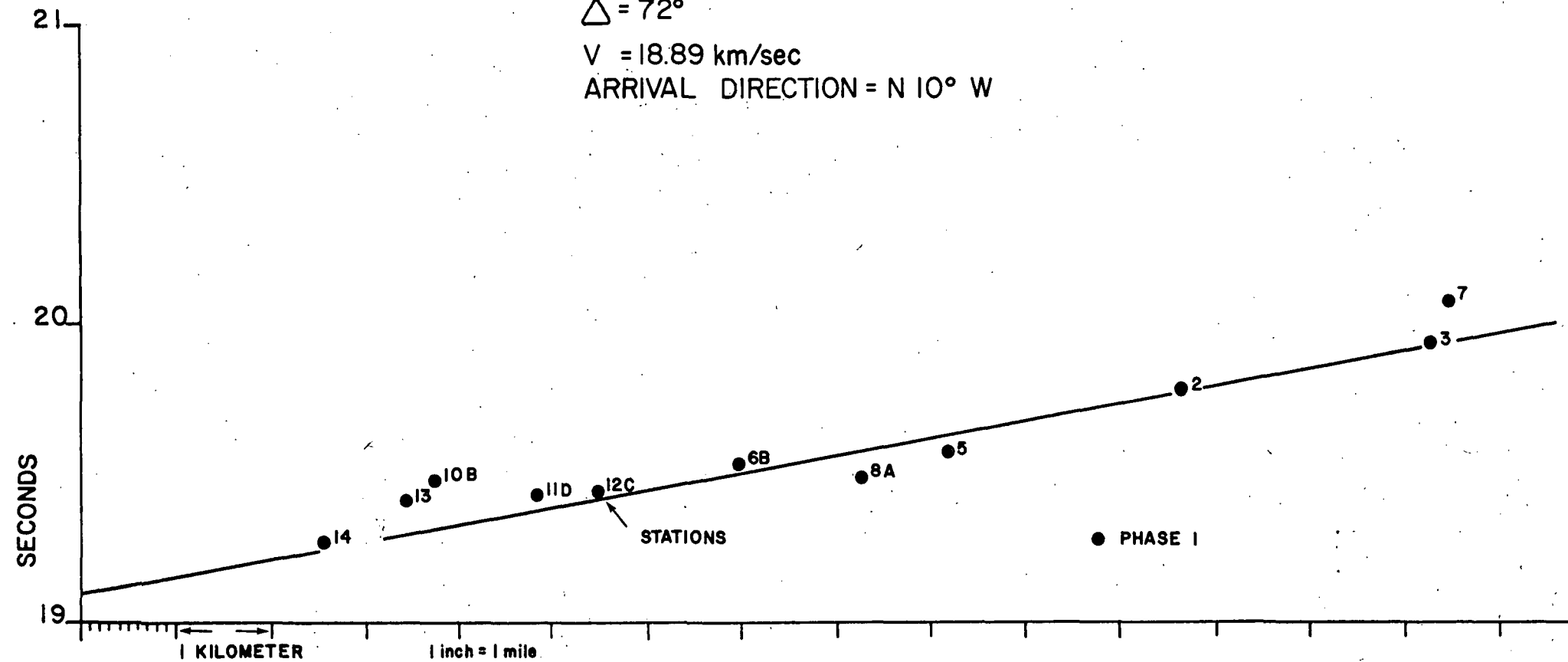
FIGURE 5.6

#7
DAY: 259   23hrs. 38 sec.
$\triangle$ = 89°
V = 23.22 km/sec
ARRIVAL DIRECTION = S 45° W

STATIONS

PHASE I

I KILOMETER   I inch = I mile
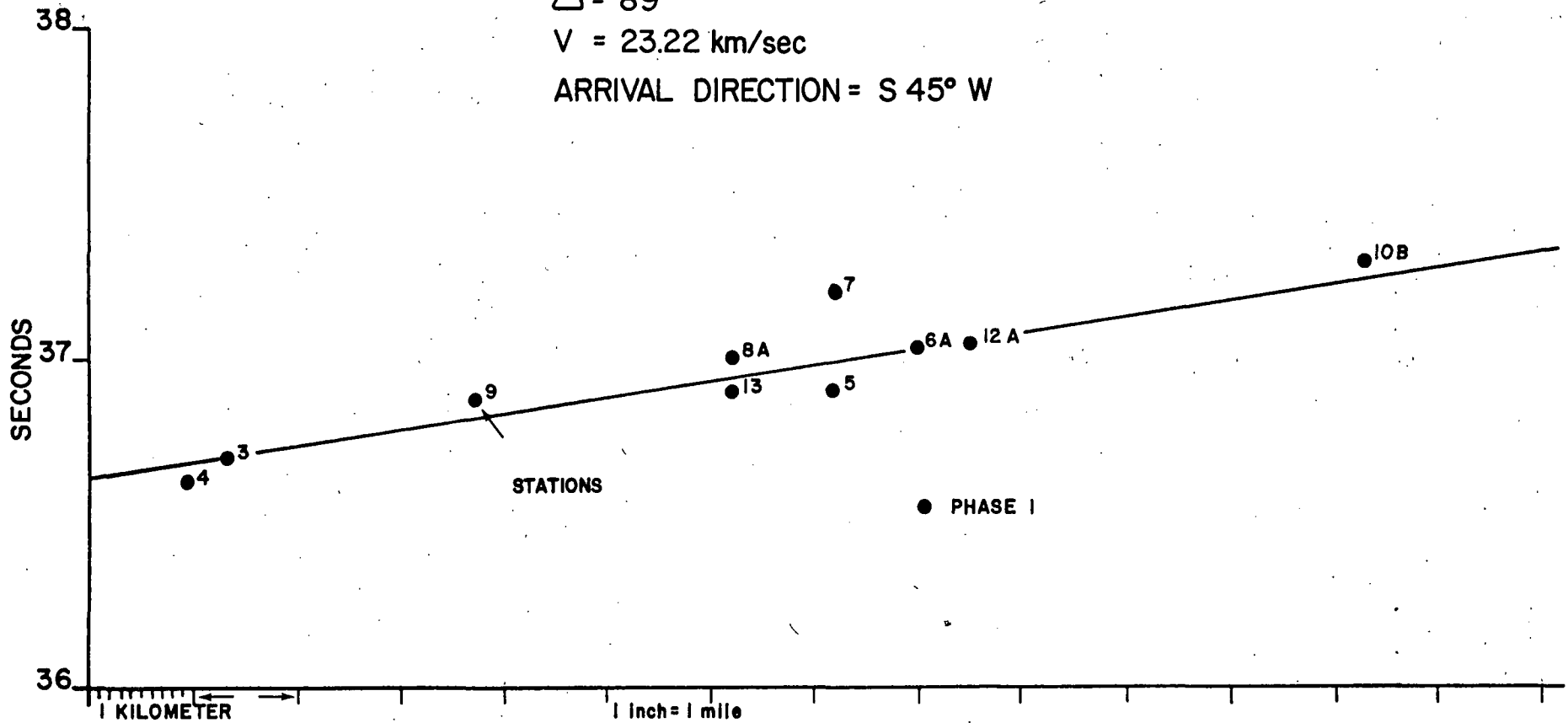
FIGURE 5.7

5.2.1   Event 1 is shown in Figure 5.1. This teleseism was recorded on 13 stations. The three phases shown represent sequential peaks and troughs in the wave form. These are picked to insure accuracy of the delay values. The largest delays are shown for stations 7 and 1 with advances at stations 14, 5, and 2. The position of the phase velocity line, however, is arbitary and was assigned to stations 13, 4, 3, 8, and 10A. These stations were interpreted to represent consistent geologic conditions.

5.2.2   Event 2 is shown in Figure 5.2. This medium distant event is a test shot from the Nevada test site. There were 6 arrivals of good quality recorded. The largest delays are shown for stations 10 and 11. An advance is shown for station 14.

5.2.3   Event 3 is shown in Figure 5.3. This teleseism was recorded on 13 stations. This event is a test shot from Russia.

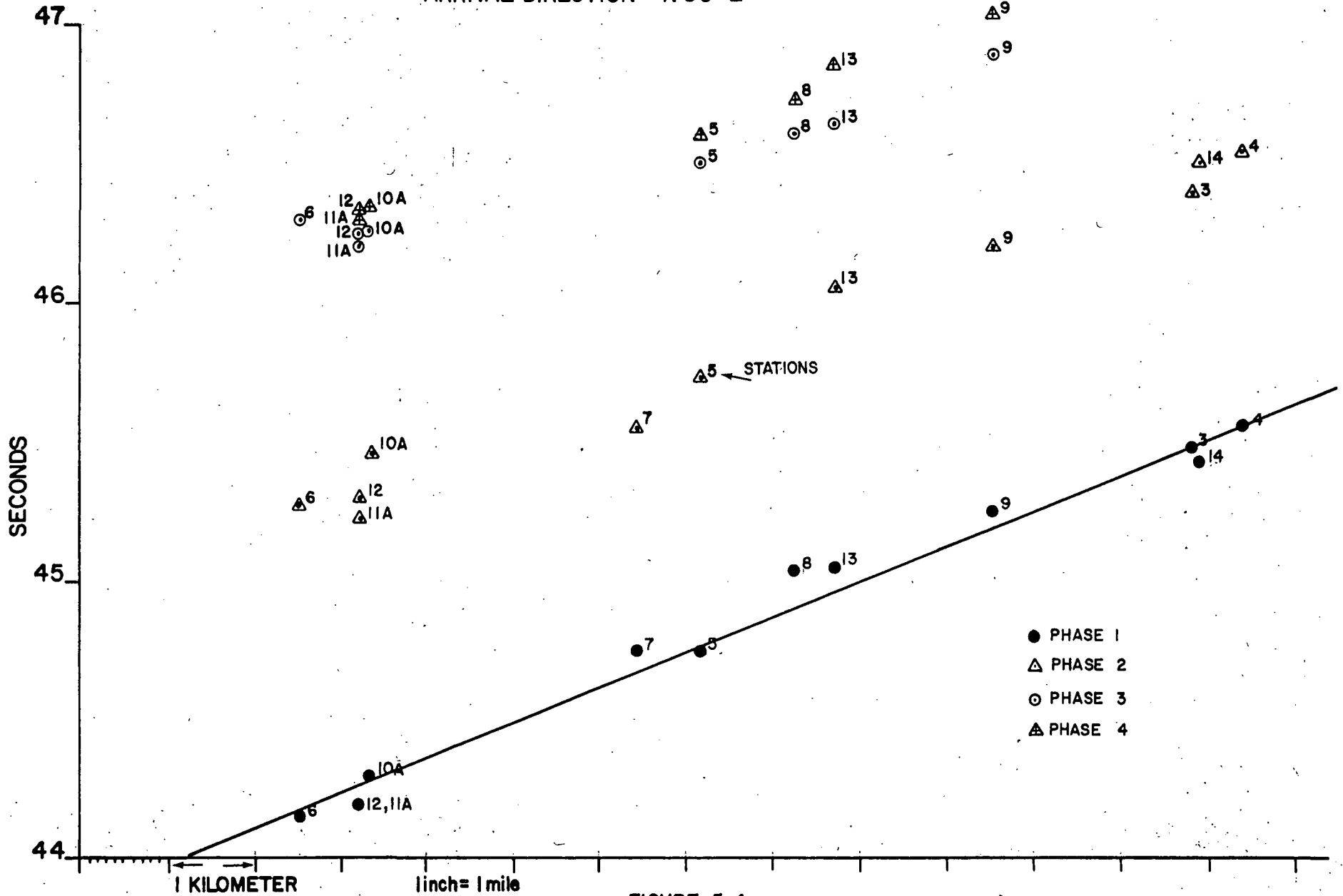5.2.4   Event 4 is shown in Figure 5.4. This event is the Snake River shot. The origin time was 11:00:05.495. The location was 42°53'54.1"N latitude and 113°48'34.2"W longitude at an altidude of 4,218 feet. The total poundage was 8,000 pounds. Three phases were picked and represent a first arrival and two reflections.

5.2.5   Event 5 is shown in Figure 5.5. This event was recorded on 10 stations.

5.2.6   Event 6 is shown in Figure 5.6. This event is an arrival from Russia and was recorded on 11 stations. Stations 7, 13, and 10B show the largest delays.

5.2.7   Event 7 is shown on Figure 5.7. This teleseism arrived in the Figi Islands and was recorded on 10 stations. Station 7 shows the largest delays.

MICROGEOPHYSICS

5.2.8 Residuals

Residuals are calculated from the psuedo refraction. The residuals are defind as the difference between an assumed plane wave and the recorded data. Plate 5.1 shows the data plotted. The station is shown as a lower hemisphere projection of the arriving ray. The values of delay or advance in milliseconds is shown adjacent to the array and example is illustrated in Figure 5.8.

5.2.9 Elevation Corrections

A surface velocity of 3.5 km/sec was assumed and a datum correction to sea level was calculated. The corrections ranged from 500 ms to 650 ms. Since the absolute level of the correction is arbitrary, then any convenient level can be used. A level to produce all delays. The resultant data map, with the elevation correction made, is shown in Plate 5.2.

5.3.0 Results

The corrected residuals are used to generate distance residuals with an assumed velocity of 3.5 km/sec. A 200 ms delay would produce "extra section" of +0.7 km along the ray path direction. The vertical section change for an emergence angle of 25° would be +0.63 km. An arbitrary depth to the velocity interface was chosen to be 2 km below sea level. This ray length then is also applied along the ray paths. Therefore, given a 25° emergence angle and a velocity delay of 200 ms, the calculated depth to the interface would be (1.81 km + 0.63 km) 2.44 km. Using this model, a reduction of the interface depth would occur for any delays less than 90 ms. Plate 5.3 is a contour map of calculated depth to the 2 km interface. This interface is approximately 3.5 km below the surface. This surface was drawn to represent the shape of the velocity structure at depth.

MICROGEOPHYSICS

P WAVE DELAY EXAMPLE

+247 (DELAY IN MILLISECONDS)

HEMISPHERE

STATION

RAY ARRIVAL AZIMUTH
WITH ERROR

D

INTERSECTION OF
WAVE RAY AND
HEMISPHERE
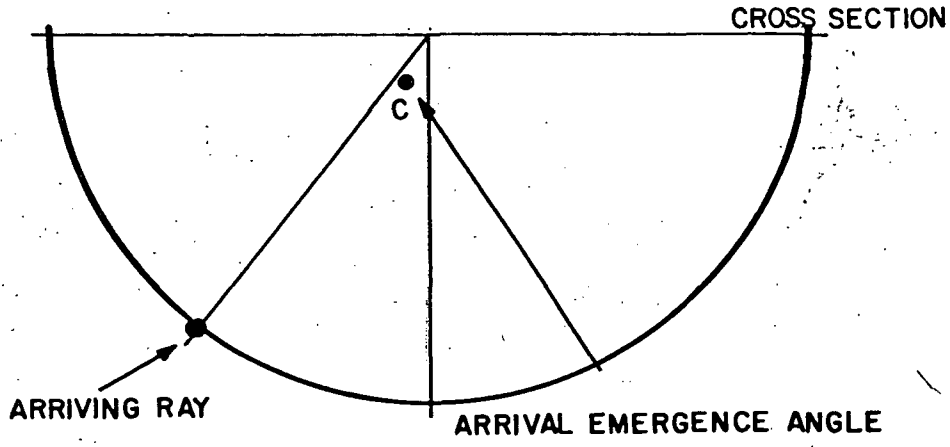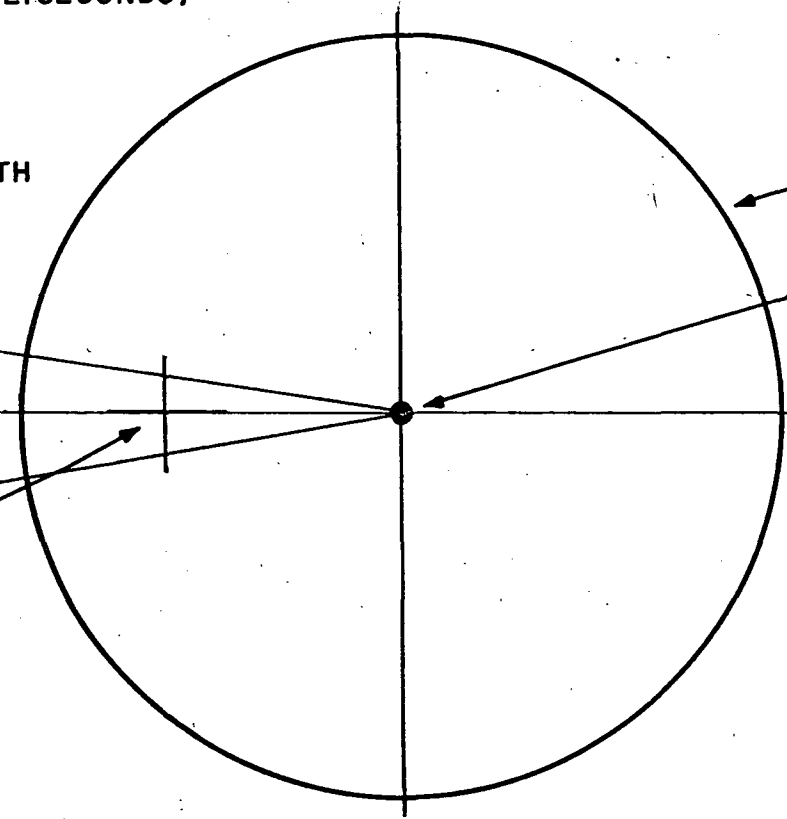
CROSS SECTION

C

ARRIVING RAY

ARRIVAL EMERGENCE ANGLE

FIGURE 5.8

5.4.0 Previous Work

Figure 5.9 illustrates the results from "crustal thickness in northern Nevada from seismic refraction profiles" plotted are the depth to the P_n interface at nearly 30 km depth. The P_n interface has ha 7.6 km/sec velocity.

5.5.0 Interpretation

The P-wave delay data show a number of results. First, the Independence Valley Basin is reflected in the large depths to the velocity interface (see Plate 5.3). Large depths to the north-west of the basin suggest that a thick section of sediments or an extension of the basin exists to the north-west of the valley to the south-west of the springs. Lastly, a high structural ridge or high velocity structure exists from the springs to the north-east. A second ridge also extends south from the springs. The P-wave data suggest that the spring area is a focus for complex velocity strucutre. These complexities may either be a result of complex faulting or alteration. Both model alternatives are favorable to the occurrence of geothermal energy.

The P-wave delay data is also consistent with the results of the previous refraction shots in the area. The Tuscarora prospect lies at a transitional point in the depth to the Maho. This major transition suggest major crustal structure trending nearly east-west through the Tuscarora property. This structure no doubt has an influence on the occurrence of geothermal energy in the northern Nevada area.

PN THICKNESS

20km
25km
30km
35km

PROSPECT

TUSCARORA

SURVEY LINES

DEPTH TO PN LAYER IN km

ELKO

BATTLE
MOUNTAIN

12 MILE

20

25

30
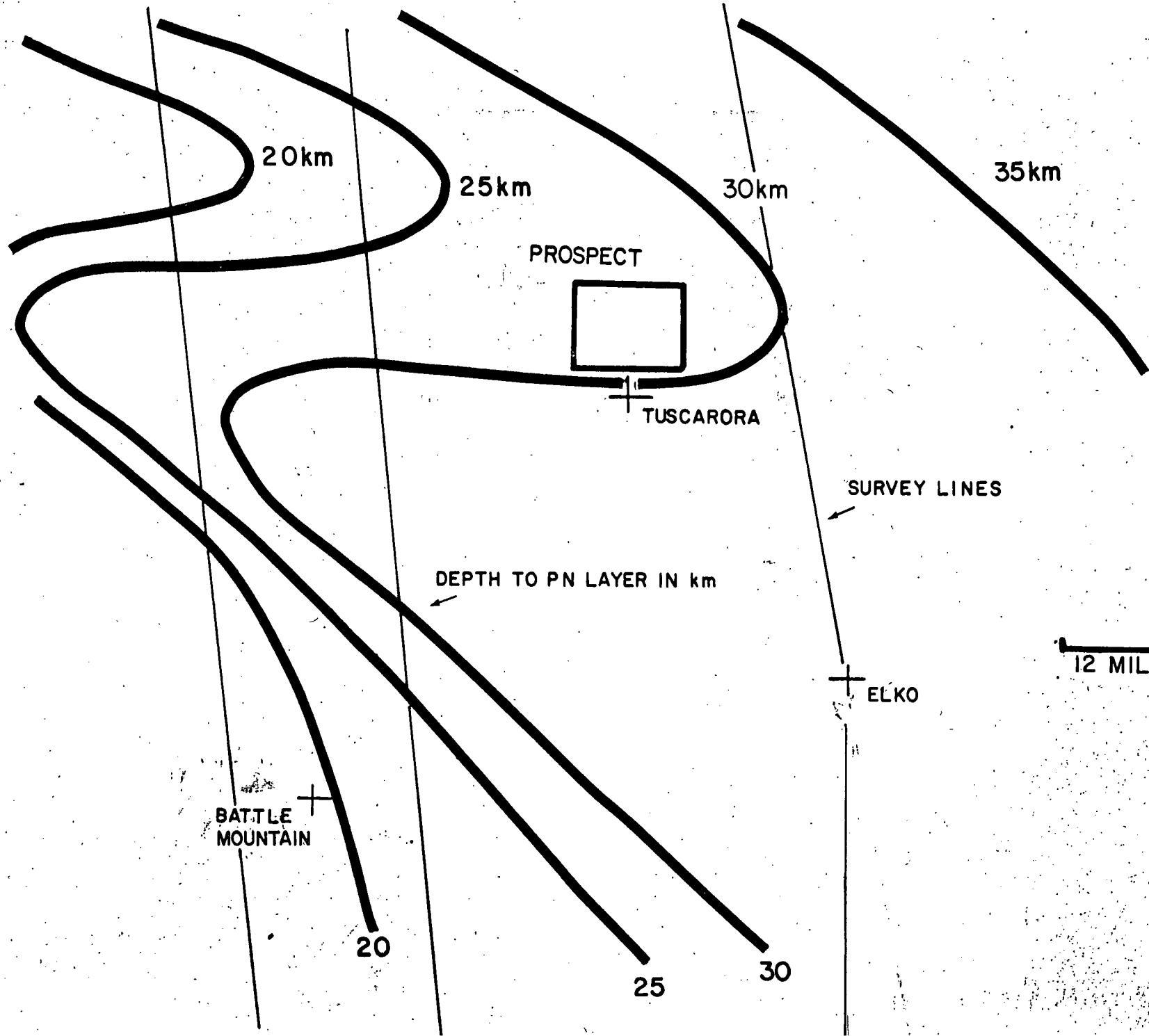
APPENDIX

PASSIVE SEISMIC METHOD

TABLE OF CONTENTS

MICROGEOPHYSICS

PASSIVE SEISMIC METHODS

Introduction

Conventional refraction and reflection seismic methods have been applied in some instances to the discovery of earth heat. However, the more widely used seismic methods are derived from classical seismology. This appendix will outline the use of the Passive Seismic Methods. The methods to be considered are the detection, location, and interpretation of the discrete seismic events called "microearthquakes", and the measurement of the velocity distribution or structural properties called "wave delay and attenuation".

MICROGEOPHYSICS

Microearthquakes

The correlation of microearthquakes and commercial geo-
thermal reservoirs is empirical. However, a high rate of seis-
micity is a sufficient ingredient in several geothermal system
models. One such model is based on the probable chemistry with-
in a convecting system. As hot water or steam rises closer to
the surface, it cools slightly and precipitates considerable ma-
terial. Without the production of fresh conduits, the system
will be plugged and the efficient convection mechanism will be
terminated. Another model simply requires a fractured medium for
deep convective circulation of meteoric waters to depths at which
the normal gradient will produce commercially useful temperatures.
In the second model, contemporary fracturing is not necessary.
However, the best evidence for the existence of fractures may be
present seismic activity.

Almost all sets of earthquakes for which magnitudes have
been measured, follow an inverse straight-line relationship be-
tween the log of the number of earthquakes and magnitude. In
general, a decrease in magnitude by 1.0 is accompanied by an in-
crease in a factor of 10 or more in the number of events occur-
ring. Thus, if the detection capability can be increased by one
magnitude, 10 or more events will be recorded for every one pre-
viously recorded. To do this, a prospect area is blanketed with
seismic stations at a nominal station spacing of 4-6 km. These
stations, recording the ground motion at displacement gains of
$1-3 \times 10^6$ at 20 Hz, will record seismic arrivals of earthquakes
down to Richter magnitude zero or below. Timing resolutions be-
tween stations is held to less than a few milliseconds and time
differences of the arrivals for any pair of stations is deter-
mined.

In order to locate an event in space, a velocity distribution
must either be assumed or determined. Most velocity models are
one dimensional with the velocity varying between constant velo-
city layers. Other models allow the velocity to increase lin-
early with depth or with vertical travel time. Ignorance of the
exact velocity model causes an accuracy problem in the computed
locations. However, precision is affected little by the velocity
model.

Microearthquake signals are dominated by frequencies be-
tween 5 to 25 Hz, making the picking of the onset somewhat sub-
jective at the ±5 ms level independent of the playback speed. This
type of error causes the location to lose precision. This error
can be controlled by a trained seismologist whose picks will be
consistent.
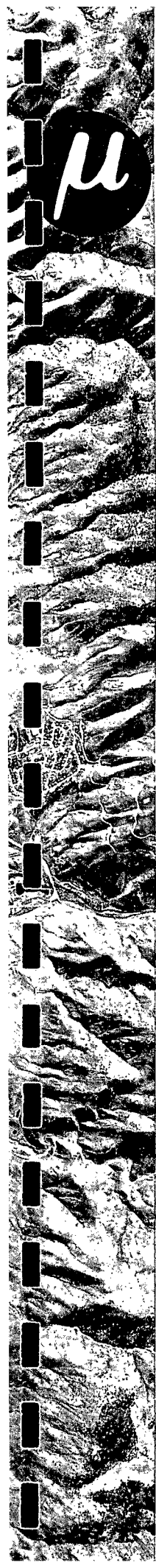
The size of the expected location error is not easily ad-
dressed. The problem is complicated by geometry, velocity mo-
dels, and geology. However, for an event recorded on eight or
more stations with a nominal station spacing 5 km and minimum
timing and velocity errors, the location should be precise to
within ±½ km in plan and ±1 in depth. Errors in the computed
location will increase outside the network of stations.

Once the event locations are finalized, their relationships with possible geology or active faulting can be made. The statistics of occurrence can also be used to characterize an area. A list of products from a microearthquake survey follows:
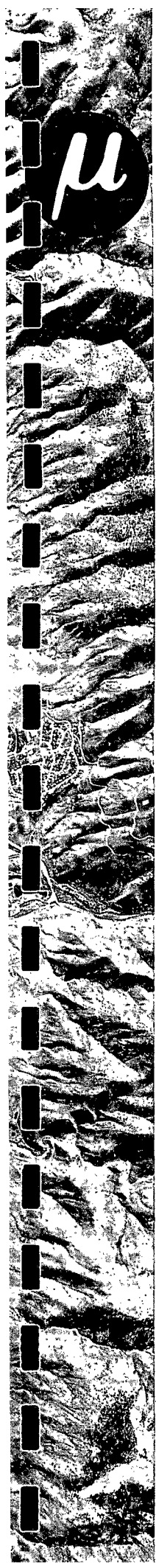
- Hypocenter Map
- Fault Plane Solutions
- Occurrence Statistics
    Event list
    Recurrence curve
    Clustering statistics (swarming)
- Rock Properties Distrubution
    Velocity distribution
    Poisson's Ratio distribution
An interpretation of the above results in terms of active fault identification and modes of deformation, identification of volumes of rock with anomalous properties, seismic safety, and recommendations.

MICROGEOPHYSICS

MICROEARTHQUAKES BIBLIOGRAPHY

Ak, Keiiti, A note on the use of microseisms in determining the shallow structures of the earth's crust (Random waves correlation earth): Geophysics, v. 30, no. 4, p. 665.

Brune, J.N., and Allen, C.R., 1976, A microearthquake survey of the San Andreas fault system in Southern California: Bull. Seismol. Soc. Am., v. 57, no. 2, p. 277-296.

Caton, P.W., 1976, Plane wave apparent velocity vector techniques for evaluating and improving location accuracies with data obtained from small arrays (7 to 10 km in diameter): Unpublished paper, 71 p.

Cheatum, C., and Combs, J., 1973, Microearthquake study of the San Jacinto Valley, Riverside County California: from the Proceedings of the Conference on Tectonic Problems of the San Andreas Fault System, p. 1-10.

Combs, J., and Hadley, D., 1977, Microearthquake investigation of the Mesa geothermal anomaly, Imperial Valley, California: Geophysics, v. 42, p. 17-33.

_____, and Robstein, Y., 1976, Microearthquake studies in the Coso geothermal area, China Lake, Califonria: Proc., 2nd U.N. Sympos. Develop. and Use of Geothermal Resources, v. 2, p. 909-916.

Crosson, R.S., 1972, Small earthquakes, structure and tectonics of the Puget Sound region: Bull. Seismol. Soc. Am., v. 62, p. 1133-1171.

Dahl, A.H., and Johnson, B.D., 1974, Preliminary results of a microseism study for the region around the Snake River Plain (1973-March 1974): Preprint presented at the Idaho Academy of Sciences, Ricks College, Rexburg, Idaho, April 19-20, 1974.

Douglas, B.M., and Ryall, A., 1972, Spectral charateristics and stress drop for microearthquakes near Fairview Peak, Nevada: Jour., Geophys. Res., v. 77, p. 351-359 .

Fitch, T., 1969, Microearthquake activity following the Parkfield, California earthquake of June 1966: Bull. Seismol. Soc. Am., v. 59, no. 2, p. 603.

Hadley, D., and Combs, J., 1974, Microearthquake distribution and mechanisms of faulting in the Fontana San Bernadino area of Southern California: Bull. Seismol. Soc. Am., v. 64, p. 1477-1499.

Hamilton, R.M., and Muffler, L.J.P., 1972, Microearthquakes at the Geysers geothermal area, California: Jour. Geophys. Research, v. 77, no. 11, p. 2081-2086.

Johnson, L.A. and Butler, D., 1975, Predicition analysis applied to microearthquake hypocenter location: abstract in Abstract and Biographies of the 45th Annual International Meeting of the Society of Exploration Geophysicists, Tulsa, Oklahoma, paper GT-15.

Kisslinger, C., and Engdahl, E.R., 1974, Semyenov Prediction, Test of the Semyenov Prediction Technique in the Central Aleutian Islands: Tectonophysics, v. 23, p. 237-246.

Knapp, R.B., and Knight, J.E., 1977, Differential thermal expansion of pore fluids: Fracture propagation and microearthquake production in hot pluton environments: Jour. Geophys. Research, v. 82, p. 2515-2522.

Lange, A.L., and Westphal, W.H., 1969, Microearthquakes near the Geysers, Sonoma County, California: Jour. Geophys. Research, v. 74, p. 4377-4378.

Langenkamp, D., and Combs, J., 1974, Microearthquake study of the Elsinore Fault Zone, Southern California: Bull. Seismol. Soc. Am., v. 64, p. 187-203.

Leslie, H.D., et al, 1976, Microearthquake location using a maximum likelihood processor: Geophysics, v. 41, no. 5, p. 960-969.

Liaw, A.L., 1977, Microseisms in geothermal exploration; studies in Grass Valley, Nevada: PhD Thesis, University of California, Berkeley, California.

Michaels, P.J., 1973, An application of the generalized linear inverse method in the location of microearthquakes and simultaneous velocity model determinations: MS Thesis, University of Utah, Salt Lake City, Utah.

Oliver, J.E., 1966, Microearthquakes: ESSA Sympos. on earthquake prediction, Rockville, Maryland, Feb. 7-9, 1966, U.S. Dept. of Commerce, Environmental Sciences Services Admin.

Pennington, W.D., Smith, R.B., and Trimble, A.B., 1974, A microearthquake survey of parts of the Snake River Plain and Central Idaho: Bull. Seismol. Soc. Am., v. 64, no. 2, p. 307-312.

Peters, D.C., and Crosson, R.S., 1973, Application of prediction analysis to hypocenter determination using a local array: Bull. Seismol. Soc. Am., v. 62, no. 3, p. 775-788.

Sanford, A.R., et al, 1976, Microearthquake investigations of magma bodies in the vicinity of Socorro, New Mexico: Geological Society of America, 1976 Annual Meeting, Denver. Abstracts: p. 1085-1086.

_____, Alptekin, O., and Toppozada, T.R., 1973, Use of reflection phases on microearthquake seismograms to map an unsual discontinuity beneath the Rio Grande Rift: Bull. Seismol. Soc. Am., v. 63, p. 2021-2034.

_____, Carapetian, A.G., and Long, L.T., 1968, High frequency microseisms from a known source: Bull. Seismol. Soc. Am., v. 58, no. 2, p. 639-644.

_____, and Singh, S., 1968, Microearthquake activity, minimum recording time for determining short-term seismicity forms: Bull. Seismol. Soc. Am., v. 58, no. 2, p. 639-944.

Spinel, R.C., et al, 1974, Microearthquake survey of median valley of the Mid-Atlantic Ridge at 360°30"N: Nature, v. 248, p. 577-579.

Steeples, D.W., and Pitt, A.M., 1976, Microearthquakes in and near Long Valley, California: Jour. Geophys. Research, v. 81, no. 5.

Ward, P.L., 1972, Microearthquakes: prospecting tool and possible hazard in the development of geothermal resources: Geothermics, v. 1, no. 1, p. 3-12.

_____, and Bjornsson, S., 1971, Microearthquakes, swarms, and the geothermal areas of Iceland: Jour. Geophys. Research, v. 76, no. 17, p. 3953-3982.

_____, and Jacob, R.H., 1971, Microearthquakes: In the Ahuachapan geothermal field, El Salvador, Central America: Science, v. 173, p. 328.

_____, Palmason, G., and Drake, C., 1969, A microearthquake survey and the Mid-Atlantic Ridge in Iceland: Jour. Geophys. Research, v. 74, p. 665-684.

Wave Delay and Attenuation

Changes in temperature affect the velocity of rock only slightly; however, the attenuation as it passes through the rock is very dependent on temperature. Fractures change the velocity to some degree, but strongly affect the ratio of P-wave and S-wave velocities. Thus, if these factors can be measured with some degree of confidence, it may be possible to isolate at least two of the requirements for a commercial reservoir, high porosity and rock at elevated temperatures.

Such experiments are best performed if an external source of seismic energy is available--either teleseismic or industrial blasting events at distances such that the received energy is approximately homogeneous. A frequency dependent transfer function between each station and master station can be calculated. The amplitude spectrum of this function will indicate the amount of attenuation taking place and the phase spectrum will indicate the time shift of the data. These values can be compared to a homogeneous model and anomalous area isolated.

The interpretation models available for P-wave and S-wave delay and attenuation studies involve either a rock property change or structural change. The attenuative models are ambiguous and no choice can be made without independent data. A list of products from a P-wave delay study follows:

- P-wave Delay Map
- S-wave Delay Map
- P-wave Attenuation Map
- S-wave Attenuation Map
- Event List
- Occurrence Statistics
- Interpretation of any anomalous velocity, structural, or attenuates with respect to potential geothermal occurrences.

MICROGEOPHYSICS

WAVE DELAY AND ATTENUATION BIBLIOGRAPHY

Eaton, G.P., Christiansen, Robert L., Iyer, H.M., Pitt, Andrew, Mabey, Don R., Blank, H. Richard, Jr., Zeitz, Isidore, and Gettings, Mark E., 1975, Magma beneath Yellowstone National Park: Science (AAAS), v. 188, no. 4190, p. 787-796.

Iyer, H.M., 1975, Anomalous delays of teleseismic P-waves in Yellowstone National Park: Nature, v. 253, no. 5491, p. 425-427.

_____, 1974, Teleseismic studies indicate existence of deep magma chambers below Yellowstone National Park: Earthquake Inf. Bull., v. 6, no. 2, p. 3-7.

_____, Evans, John R., and Coakley, John, 1974, Teleseismic evidence for the existence of low-velocity material deep into the upper mantle under Yellowstone Caldera: EOS (Am. Geophys. Union Trans.), v. 56, no. 12, p. 1190.

Pitt, A.M., 1974, Evidence from local earthquakes for the existence of a region of seismic body wave attenuation in the upper crust under the Yellowstone Caldera: EOS (Am. Geophys. Union Trans.), v. 56, no. 12, p. 1190.

Steeples, Don W., and Iyer, H.M., 1975, Location and estimation of volumes of anomalously hot material beneath some geothermal areas from teleseismic P-delays: U.N. Sympos. Develop. and Use of Geoth. Res. Abst., no. 2.

INSTRUMENTATION

Introduction

The passive seismic system used for geothermal exploration and deployed by MicroGeophysics Corporation (MGC) is a hybrid system. The system consists of both independent seismographs and RF telemetered stations. The network station capability is from six to ten stations. A schematic of the system is shown in Figure 1. The independent stations are basically MEQ-800 visual drum recorders, with an integral timing system synchronized to universal coordinated time. As an option, the seismic signal can also be recorded by a continuous magnetic tape recorder. This independent station schematic is shown in Figure 1. The RF-telemetry system consists of from two to eight satellite stations with a central recording system. The satellite stations are comprised of a geophone, amplified voltage controlled oscillator with a RF transmitter.

The central system receives data from each of the satellite stations, discriminates them, and records them. The recording can be on smoked paper, and/or magnetic tape, and/or event recording on a high speed photographic recording. A schematic is shown in Figure 1. A detailed explanation of each of the component parts for each system is given in the following sections.

L4-C Seismometer

The L4-C is a one-Hertz-natural-frequency vertical seismometer (manufactured by Mark Products). The damping is 0.6 of critical damping. The L4-C has an output of 6.9 volts per inch/second. A typical specification sheet is shown in Figure 2.

As sensor options, other geophones can be utilized. A common option is the L-10 geophone (manufactured by Mark Products). A typical specification sheet is also shown in Figure 2.

MEQ-800-B

The MEQ-800-B is a visual microearhtquake recorder. The smoked drum recording has a nominal 120 mm/min rotation speed with 1 mm spacing between succeeding traces. The stylus and trace width is 0.05 mm. The amplifier has a maximum of 120 db of gain and selectable corners at 1, 5, and 10 Hz. The high cut filter has selectable corners of 10, 20, and 75 Hz. The amplifier gains can be changed by precise 6 db steps down from 120 db. The maximum pen deflection is ±25 mm and can be limited under severe ground noise conditions to ±10 mm or ±5 mm.

The integral timing system consists of a clock, whose drift rate is less than ±1 part in 10^7 (approximately ±10 ms per day) and can be set to standard time and adjusted at 16 ms increments. Time is displayed on each trace by a slight deflection of the pen each second.

MICROGEOPHYSICS

SYSTEM SCHEMATIC

INDEPENDENT STATIONS

4-5 Stations Available
Remote Station Location

Components:

   Geophone
     ↓
   Amplifier
     ↓
   Filters
     ↓
 *Recorder
    Smoked Paper
    Digital Tape (optional)

TELEMETRY STATIONS

4-5 Stations Available
Remote Station Location

Components:

   Geophone
     ↓
   Amplifier
     ↓
   Filter
     ↓
   Voltage Controlled
   Oscillator (VCO)
     ↓
   RF Transmitter

CENTRAL STATION

Components:
  RF Receiver

  Discriminator

 *Recorder
    Smoked Paper
    Event Detection
    Digital Tape

*Timing supplied by each station, synchronized daily.

FIGURE 1

MICROGEOPHYSICS

L4-C SPECIFICATIONS

Open Circuit Damping $(b_o) = 0.28$ Critical

Coil Current Damping $(b_c) = \dfrac{1.1\ R_c}{R_c + R_s}$

Total Damping $(b_t) = b_o + b_c$

L-4C 1.0 Hz GEOPHONE

Coil Resistance (ohms)	84	134	206	320	500	870	1280	2000	3500	5500
Transduction (volts/inch/sec.)	0.87	1.13	1.34	1.7	2.1	2.8	3.5	4.2	5.55	6.9
Transduction (volts/meter/sec.)	34.2	43.5	53	67	83	110	136	165	220	273
Coil Inductance (henries)	0.092	0.147	0.230	0.35	0.55	0.95	1.40	2.20	3.85	6.05
Analog Capacity (microfarads)	875	550	356	230	147	85	58	37	21	13.4
Analog Inductance (henries)	29	46.4	71	110	173	300	440	690	1200	1900
Shunt For 0.70 Critical Damping	133	215	333	520	810	1400	2070	3250	5650	8900
Shunt For 0.60 Critical Damping	205	325	500	780	1220	2120	3100	4900	8500	13400

L-4C 1.0 Hz GEOPHONE

TYPE	Moving dual coil, humbuck wound
FREQUENCY	1.0 ± 0.05 Hz measured on 200 pound weight at 0.09 inches/second.
FREQUENCY CHANGE WITH TILT	Less than 0.05 Hz at 5° from vertical.
FREQUENCY CHANGE WITH EXCITATION	Less than 0.05 Hz from 0 to 0.09 inches/second
SUSPENDED MASS	1000 grams
STANDARD COIL RESISTANCES	See Table
LEAKAGE TO CASE	100 megohm minimum at 500 volts
TRANSDUCTION POWER	$8.8 \cdot 10^3$ watts inch second or 13.6 watts meter second
OPEN CIRCUIT DAMPING	$(b_o) = 0.28$ critical
CURRENT DAMPING	$(b_c) = \dfrac{1.1\ R_c}{R_s - R_c}$
	where: $R_c =$ coil resistance - ohms $R_s =$ shunt resistance - ohms
COIL INDUCTANCE	$(L_c = 0.0011\ R_c$ L_c in in henries.
ELECTRIC ANALOG OF CAPACITY	$C_c = \dfrac{73.500}{R_c}$ (microfarads)
ELECTRIC ANALOG OF INDUCTANCE	$L_m = 0.345 R_c$ (henries)
CASE HEIGHT	5⅛ inches — 13 cm.
CASE DIAMETER	3 inches — 7.6 cm.
TOTAL DENSITY	3.7 grams cm³
TOTAL WEIGHT	4¾ pounds — 2.15 kilograms
OPERATING TEMPERATURE	Range: −20° to 140°F or - 29 to 60 C.
OPERATING PRESSURE	500 PSI.
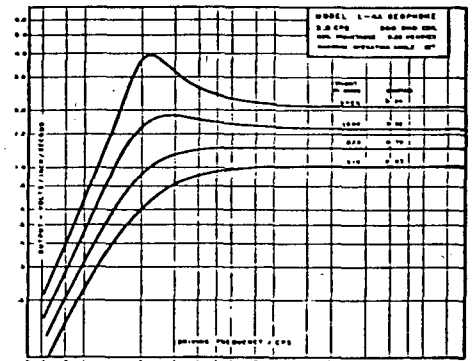
L-10A SPECIFICATIONS

L-10A GEOPHONE

Suspended Mass (m) .... 12.5 grams

Open Circuit Damping (b_o) .... $b_o = \dfrac{4.2}{f} \pm 10\%$

Coil Circuit Damping (b_c) .... $b_c = \dfrac{15.7 \cdot R_c}{f(R_s + R_c)} \pm 10\%$

Analog Capacitance (C_c) .... $C_c = \dfrac{5010}{R_c}$

$\quad R_c =$ Coil Resistance $\quad\quad C_c =$ Microfarads

Analog Inductance (L_m) .... $L_m = \dfrac{5.16 \cdot R_c}{f^2}$

$\quad f =$ geophone frequency $\quad L_m =$ henries

L-10B 4.5Hz

Coil Resistance (ohms)	21	34	54	90	138	215	374	590	940
Transduction (volts/inch/second)	0.193	0.245	0.30	0.387	0.49	0.60	0.80	0.98	1.25
Coil Inductance (henries)	0.004	0.006	0.010	0.016	0.024	0.038	0.067	0.105	0.167
Analog Capacitance (micro farads)	350	216	136	81.6	53.1	34.1	19.7	12.4	7.80
Analog Inductance (henries)	3.58	5.82	9.24	15.4	23.6	36.8	64.0	102	161
Shunt for 1.00 Critical Damping (ohms)	66.8	108.5	173	277	317	687	1200	1890	3000
Shunt for 0.70 Critical Damping (ohms)	191	311	494	824	1260	1750	3420	5410	8570
Shunt for 0.60 Critical Damping (ohms)	315	512	814	1355	2080	3240	5640	8910	10425

$b_o = .445 \qquad b_c = \dfrac{2.33\ R_c}{R_c + R_s}$

L-10B GEOPHONE

Suspended Mass (m) .... $m = 19$ grams

Open Circuit Damping (b_o) .... $b_o = \dfrac{2}{f} \pm 10\%$

Coil Circuit Damping (b_c) .... $b_c = \dfrac{10.5 \cdot R_c}{f(R_s + R_c)} \pm 10\%$

Analog Capacitance (C_c) .... $C_c = \dfrac{7330}{R_c}$

$\quad R_c =$ Coil Resistance $\quad\quad C_c =$ Microfarads

Analog Inductance (L_m) .... $L_m = \dfrac{3.41 \cdot R_c}{f^2}$

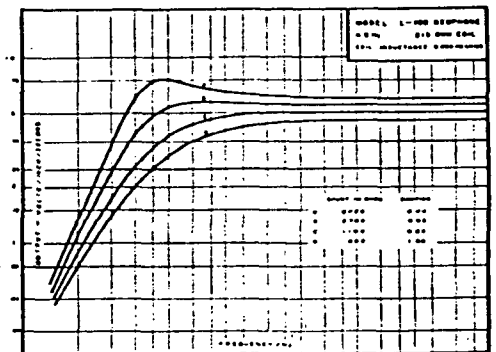$\quad f =$ geophone frequency $\quad\quad L_m =$ henries
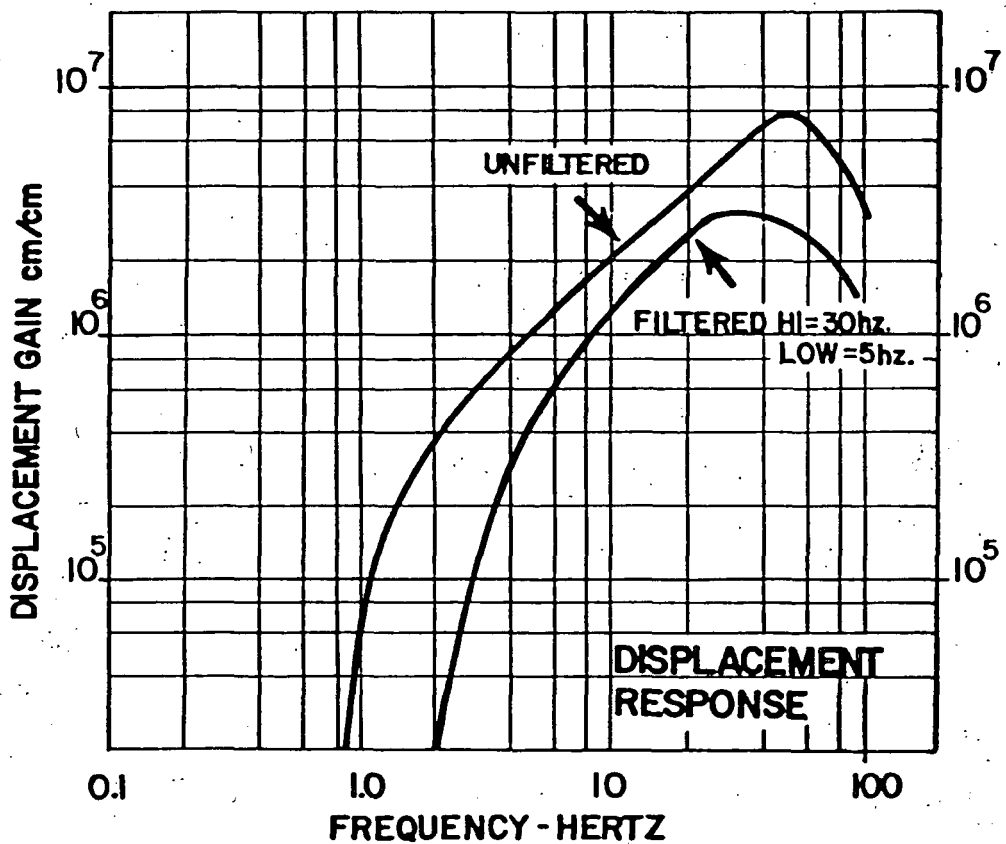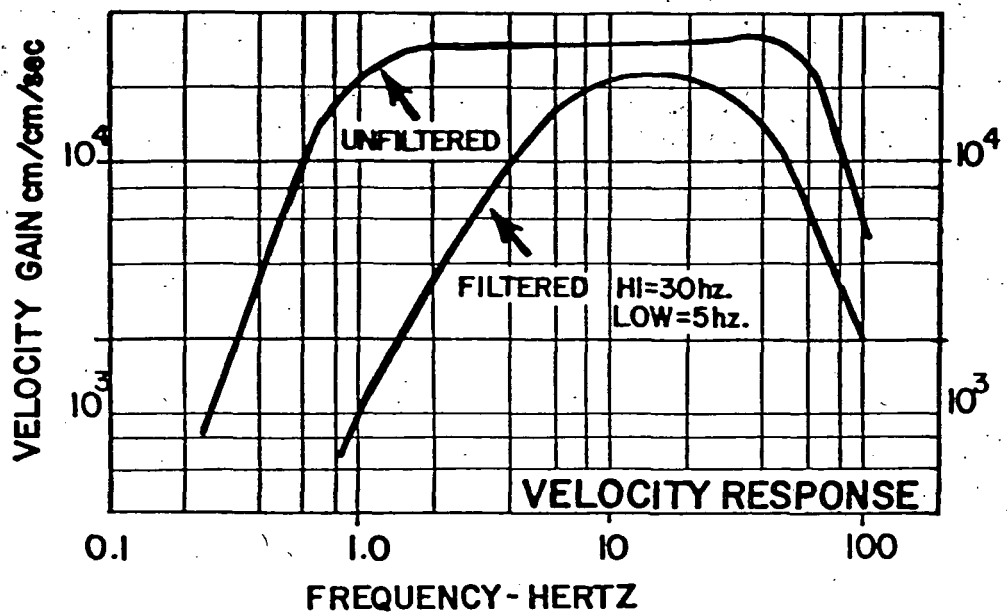

FIGURE 2

INSTRUMENT RESPONSE

FIGURE 3

The frequency characteristics of the instrument with an L4-C are summarized in Figure 3. Both the velocity and displacement response for the MEQ-800-B microearthquake system are shown. The displacement response at a particular frequency (f) can be calculated by multiplying the velocity gain at f time $2\pi f$. The filter response and gain level shown are typical settings for operations in the western continental United States.

DMTR

The digital magnetic tape recorder (DMTR) is a twelve-bit 100 sampler-per-second, reel-to-reel-tape recorder which records data continuously. Each data block begins on the minute at the command of the clock in the MEQ-800-B system. The hour and minute from the clock are written at the beginning of each block. WWVB is recorded continuously on one bit of the tape format. The dynamic range of 72 db on this tape recorder allows the recovery of data under exceptionally noisy conditions.

WWVB

WWVB is the radio call code for the National Bureau of Standards 60 kHz time-standard station in Fort collins, Colorado. The WWVB time standard is used to set and synchronize the microearthquake system clocks. As shown in Figure 4 below, the signal consists of 60 markers each one minute, with one marker each second (time progresses from left to right). Each marker is generated by reducing the power of the carrier by 10 db at the beginning of the corresponding second and restoring it:

(1) 0.2 seconds later for a binary zero
(2) 0.5 seconds later for a binary one
(3) 0.8 seconds later for a 10 second position marker and for a minute reference marker.

TIME FRAME 1 MINUTE
(INDEX COUNT 1 SECOND)

0   10   20   30   40   50   0

Point A is 258 Days, 18 hours, 42 minutes and 36 seconds.

ON TIME

POINT A

P₀   P₁   P₂   POINT A   P₃   P₄   P₅   P₆

0.3 SECOND   0.2 SECOND   W   U   0.5 SECOND   0.8 SECOND

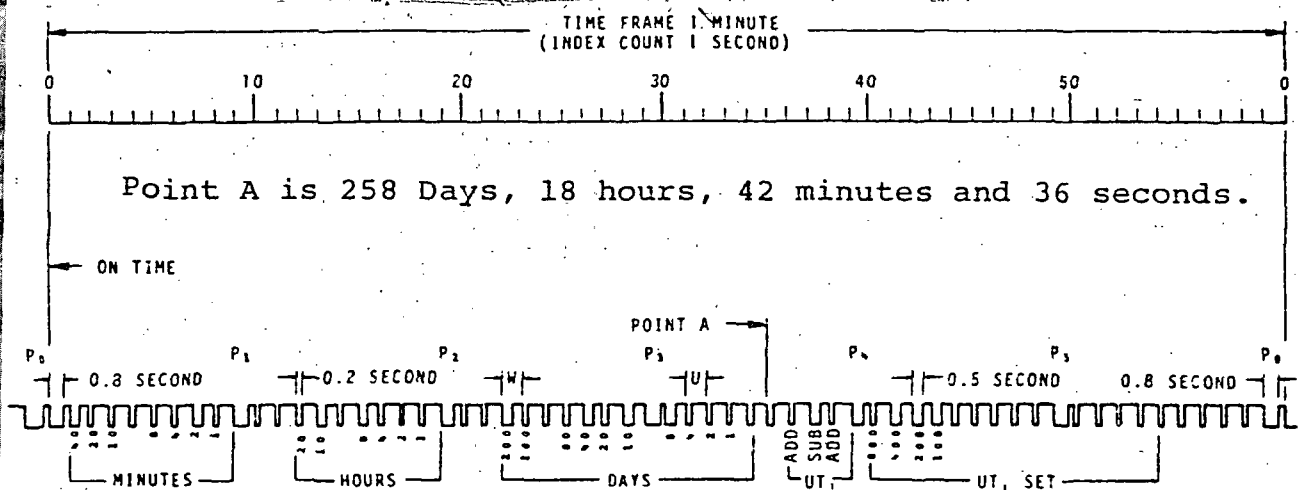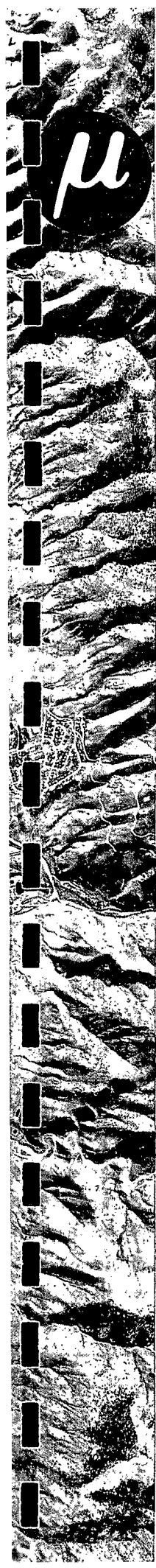MINUTES   HOURS   DAYS   UT   UT SET

FIGURE 4

The WWVB code (as shown in Figure 3) is recorded daily on the visual drum as absolute time and date identification of the record, and is used to synchronize each MEQ system to standard time.

The MEQ systems' clocks are synchronized daily with WWVB by comparing (on an oscilloscope) the beginning of the WWVB second pulse with the MEQ-800-B internally generated one-second pulse. This comparison can be done to ±2 milliseconds. Daily records are kept on the amount of correction for each clock. These time corrections are then applied to the records. Common corrections are on the order of 15 ms per day or less than one millisecond per hour.

WWV

WWV is the radio call code for the National Bureau of Standards 5, 10, 15, 25 mHz time standard station in Fort Collins, Colorado, as used by MicroGeophysics Corporation. The voice channel is used to generally coordinate time, while the second signals are used to precisely coordinate time. The use is similar to that of the WWVB channel.

Amplifier

The amplifier used is the AS-110 (manufactured by Sprengnether Instrument Company). This amplifier has identical characteristics to the Sprengnether MEQ-800 amplifier.

Telemetry

The following are excerpts for the Sprengnether Manual for the VCO and Discriminator equipment:

Telemetry VCO   TC-10

The TC-10 Voltage Controlled Oscillator has been designed to fill a need for low cost, low power, high quality and versatile audio frequency telementry components. Available in standard constant bandwidth channels from 340 to 3060 Hz with ±125 Hz deviation the TC-10 VCO satisfies requirements for FM geophysical data telemetry in the frequency range DC to 50 Hz by telephone, land line, or by radio link. When used with the companion TC-20 Discriminator, 60 dB dynamic range (peak measurement is achieved in the 0-10 Hz bandwidth.

Versatility and simplicity of installation are assured by several special features incorporated into the VCO that are not normally available at such low cost. Eleven sensitivity ranges, from

50 mv to 100 v full scale deviation, are selectable
on the front panel to facilitate system gain ad-
justments or multi-gain operations. Upper and
lower band edge deviations can be effected from a
front panel switch for ease in system setup and
servicing. Center frequency, deviation, and out-
put level can be monitored and adjusted from the
front panel. Output is tranformer coupled for
flexible installation.

Power requirements are generous at ±10 to 15
VDC at 15 ma for low power remote field instal-
lations. Small physical size is ideal for com-
pact field case installation (the TC-10 matches
the AS-110 amplifier in size and connector con-
figuration) or for high density packing in rack
mount multi-channel operations.

The TC-110 VCO represents state-of-the-art in
circuit design, user convenience, and low price,
satisfying virtually all requirements for high
quality audio frequency FM telemetry.

Discriminator TC-20

The TC-20 Discriminator has been designed to fill
a need for low cost, low power, high quality and
versatile audio frequency telemetry components.
Available in standard constant bandwidth channels
from 340 to 3060 Hz with ±125 Hz deviation the
TC-20 satisfies requirements for FM telemetry of
geophysical data in the frequency range DC to
50 Hz by telephone or land line or by radio link.
When used with the companion TC-10 VCO, 60 dB
dynamic range (peak measurement) is achieved in
the 0-10 Hz bandwidth.

Several unique features are found on this low
cost phase-locked loop discriminator that nor-
mally are incorporated only in more expensive
units. A sense light on the front panel indi-
cates low carrier level. Provision is made for
a reference compensation tone and trim to effect
compensation for frequency shifts in multiplexed
tone bundles. The TC-20 also provides for an
auxiliary-test input on the front panel to faci-
litate service checks and adjustments. The
carrier after filtering can be monitored from
the front panel and all major adjustments are
made with front panel controls. The input is
transformer coupled for flexibility in installa-
tion.

MICROGEOPHYSICS

Power requirements are ±10 to 15 VDC at 18 ma.
Output filters (3 pole Butterworth) at 1, 5, 10,
20, 50 Hz (3dB) are available, factory adjusted.
The panel width of 1-1/2" allows dense packing
in rack installations.

The TC-20 represents state-of-the-art in phase-
locked loop discriminators, offering the maximum
in flexibility and convenience features at the
lowest possible cost.

RF Telemetry Link

These RF telemetry links are Monitron low-power FR transmit-
ters and receivers (manufacturer Monitron Corporation). The out-
put power is less than 100 mw. Specifications are shown below.

System Gains: The typical gains of each system with typical set-
tings are shown below:

System: MEQ-800 (Smoked Paper)

   Filter Settings:
    Hi = 30 Hz
    Lo = 5 Hz
   Geophone L4-C

Gain Settings	Displacement Gain at 20 Hz
60	0.04×10^6
66	0.08×10^6
72	0.16×10^6
78	0.33×10^6
84	0.165×10^6
90	0.3×10^6
96	2.6×10^6
102	5.2×10^6

System: VCO-TELEMETRY-VR-60

   Filter Settings   VCO = 5 Volts/f.s.
    Hi = 30 Hz   VR-60 + 100 mu/mm
    Lo = 5 Hz
   Geophone L4-C

| Gains Settings	Displacement Gain at 20 Hz
60	0.2×10^6
66	0.4×10^6
72	0.8×10^6
78	1.65×10^6
84	3.25×10^6
90	6.5×10^6
96	13.0×10^6
102	26.0×10^6

MICROGEOPHYSICS

DATA

An example of the output of a microearthquake system is shown in Figure 6. The smoked-paper output is shown in Figure 6(a) while Figure 6(b) and Figure 6(c) are the same earthquake recorded on magnetic tape and played back at two different speeds. The playback format is illustrated in the figure.

The smoked-paper record is used at the time of the recording (in the field) to estimate the seismicity and to locate any recorded microearthquake approximately. The paper records can be picked under magnification to a precision of less than ±30 ms. The magnetic tape playbacks are then used to increase the timing precision of an event to ±10 ms, a precision close to the subjective level of interpretation by an experienced seismologist. The magnetic tape playbacks are also useful in increasing the effective gain of recording and thereby recording very small amplitude events. In noisy areas, the tape playbacks can be used to recover data obscured on the paper monitor records by cultural noise on adjacent traces.

5a

1.0 MIN

5b
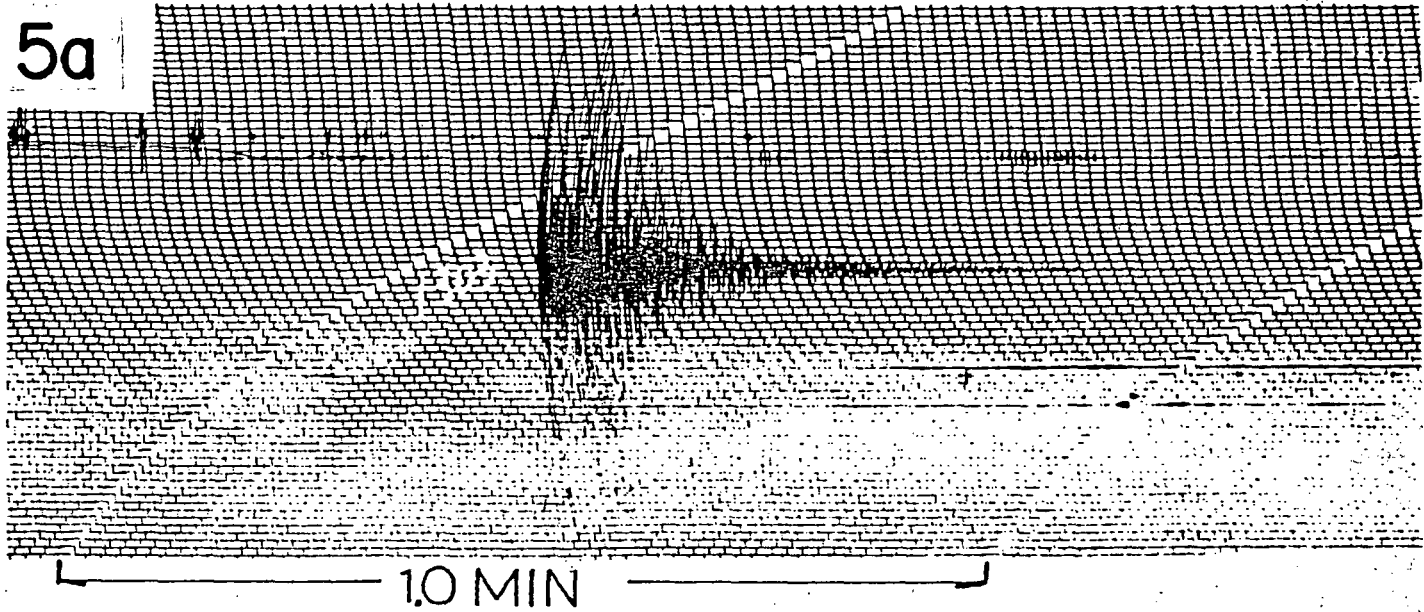
MI424.R04

Plot gain in db above station gain

STATION NUMBER —————— 3
GAIN IN db —————————— 90
TIME (DAY,HOUR,MIN)—— 159 13 3
STARTING SEC ————————— 5.000
DRUM SPEED (MM/SEC)—— DRMSPD: 7.00

0.51

5.000

1.0 SEC

5c

MI424.R04

FIRST BREAK

3
90

159 13 3
5.000

DRMSPD: 40.00

0.22

1.0 SEC

0.000

Micro Geophysics